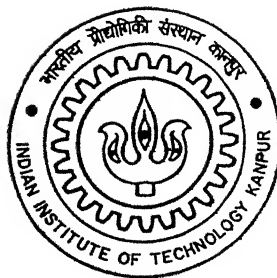# Modeling and Experimental Anaylsis on Extrudate Swell of Polyethylene, Polypropylene and Polystyrene
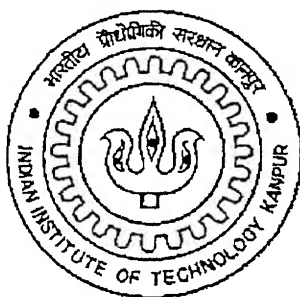
by

Sanjay Gupta

MATERIALS SCIENCE PROGRAMME

Indian Institute of Technology Kanpur

DECEMBER, 2002

MODELING AND EXPERIMENTAL ANAYLSIS ON EXTRUDATE SWELL OF POLYETHYLENE, POLYPROPYLENE AND POLYSTYRENE

A thesis submitted
in partial fulfillment of the requirements
for the Degree of

Master of Technology

-By

Sanjay Gupta

Materials Science Programme

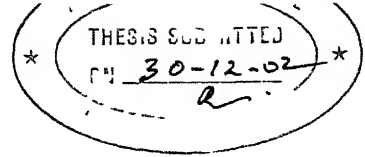**Indian Institute of Technology, Kanpur**

December, 2002

CERTIFICATE

THESIS SUBMITTED 30-12-02

This is to certify that the work presented in the thesis entitled *"**Modeling and experimental analysis on extrudate swell of polyethylene, polypropylene and polystyrene**"*, that is being submitted by Mr Sanjay Gupta for the award of degree of Mater of Technology to the Indian Institute of Technology Kanpur is bonafide research work carried out by him under my supervision and guidance.

Mr Gupta has worked on this problem for about a year In opinion, the thesis has reached the standard and the requirement of the institute The results embodied in the thesis have not be submitted for the award of any other degree or diploma

IIT Kanpur

December, 2002

(Dr. Kamal K Kar)

Thesis Supervisor

Materials science Programme

IIT Kanpur

ACKNOWLEDGEMENT

I am deeply indebted to Dr Kamal K Kar who guided and inspired me, giving confidence and enthusiasm in a situation of patience and concentration He has been a constant source of inspiration with never give up attitude. It is a nice experience to work with him The way he made me think and work has an everlasting impact on my career I am expressing my sincere thanks to him who helped me to make this moment a memorable one

I am grateful to all my lab mates Balram Dewangan, Praveendra Pratap Singh, and Pradeep Paik for their cooperation, suggestion and encouragement throughout my work

I am thankful to my friends Ashish Kumar Sharma, Dhananjay Kumar Srivastava, R Santosh Rao, Tathagata Bhattacharya, Rahul Dubey, Sandesh Gupta, Nitin Khanna, Amit shraivastava, D Satish, Pramod Kumar Gupta, Rajiv Mishra and Anand Biswas for constantly helping me and making my stay at IITK a memorable one

Last but not the least, from the bottom of my heart I am deeply indebted to my parents, sisters, and brother for their ceaseless inspiration and constant encouragement

It would be perfidious on my part, if I fail to express my sincere thanks to God for his constant inspiration

I I T Kanpur
December, 2002

Sanjay Gupta

ABSTRACT

Rheological properties like viscosity, shear stress and first normal stress difference of low density polyethylene, polypropylene and polystyrene (both amorphous and crystalline) under steady shear condition have been investigated in advanced rheometric expansion system (ARES) rheometer over a wide range of shear rate and processing temperature. Viscosity decreases with an increase of shear rate for low density polyethylene, polypropylene and polystyrene (both amorphous and crystalline) But first normal stress difference and shear stress increases with increasing shear rate for both these materials These rheological properties are analyzed with Power law (1925), Bueche (1962), Cross (1965), Ellis (1977), Carreau (1979), Bingham (1922), Herschel and Bulkley (1926), Casson (1959), Ferry (1942), Spencer and Dillon (1949) and Berger's model (1998) Die swell measurements are also performed on these materials in a Randcastle microtruder over a range of shear rate and polymer melt temperatures to accelerate efforts to develop reliable quantitative description of die swell phenomenon observed in practical polymer processing operations Die swell of these polymers increases with increasing shear rates. But an increase in polymer melt temperature decreases the die swell of polymers A comparison of the experimental data with predictions from various existing models such as the ones reported by Tanner (1970), Bagley and Duffy (1970), Mendelson et al (1971), White and Roman (1976, 1977), Vinogradov and Malkin (1980), Macosko (1990) and Kumar et al (1992) reveals that existing models are not capable of accurately predicting the die swell of the materials Only Macosko model (1990) shows some agreement. Therefore a theoretical model based on first normal stress difference, shear

rate, relaxation time and other processing parameters with no adjustable parameters appropriate for determining die swell has been developed for these materials The experimental data for the polymers studied confirms excellent well with predictions from this proposed model

CONTENTS

Chapter 3

Proposed model

Chapter 4

Results and discussion

Chapter 5

5. SUMMARY AND CONCLUSIONS

REFERENCES

LIST OF FIGURES

LIST OF TABLES

LIST OF SYMBOL

B	die swell
N_1	first normal stress difference (Pa)
N_2	second normal stress difference (Pa)
τ_w	wall shear stress (Pa)
G	elastic modulus in shear (Pa)
γ	shear rate (s^{-1})
L	length of the die (mm)
D	diameter of the die (mm)
S_R	recoverable shear strain
De	Deboarh number
ρ	density of the fluid (Kg/m^3)
η	viscosity of the fluid (N-s/m^2)
v	average velocity of the flow (mm/sec)
θ	die entrance angle (theta)
M_w	molecular weight
MWD	molecular weight distribution
Δp	pressure drop across the die (Pa)
α_T	time-temperature shift factor
t_n	relaxation time at glass transition temperature (s)
t_n^{*}	relaxation time at a particular temperature (s)
B	Finger strain tensor
I_B	trace of matrix B
C^{-1}	Cauchy strain tensor
I_C	trace of matrix C^{-1}

δ_{ij}	Kronecker delta or identity matrix
T	stress tensor
P	hydrostatic pressure (Pa)
U	function of B, C, t, and t'
F_o	deformation gradient
F	relative deformation gradient
$F^{(v)}$	viscometric history gradient
τ_{zz}	shear stress in the direction of flow (Pa)
F^T	transpose of relative deformation gradient
Q	transformation matrix
c_1, c_2	WLF equation constants
T	temperature (K)
T_g	glass transition temperature (K)
t	time in to consideration (s)
t'	time in the past (s)
α_1	extension in the flow direction
α_2	extension in the radial direction
R	regression coefficient

CHAPTER 1
INTRODUCTION

The elastic nature of polymer melt is shown in extrusion processes by the phenomenon of die swell, alternately termed "extrudate swell", "memory", "puff-up", or "Barus- Effect" in which the extrudate diameter is much greater than the diameter of die [1]. This effect is often described experimentally by giving a "swelling index", B found as the ratio of the extrudate diameter to the die diameter, which is represented by

$$B = (D_f/D_i) \qquad\qquad \dots (1.1)$$

where B, D_f and D_i are the die swell, extrudate diameter and die diameter respectively. This is also shown in Fig. 1.1.

If the flow channel is noncircular, the extrudate will also undergo a change of shape [1]. In such cases more than one swelling ratios are to be used [2]. The problem of die swell and characterization of melt emerging from dies have been of considerable concern in the polymer industry for more than half-century. Most of the studies have involved flow through capillary dies and indeed only few investigators have reported this phenomenon.
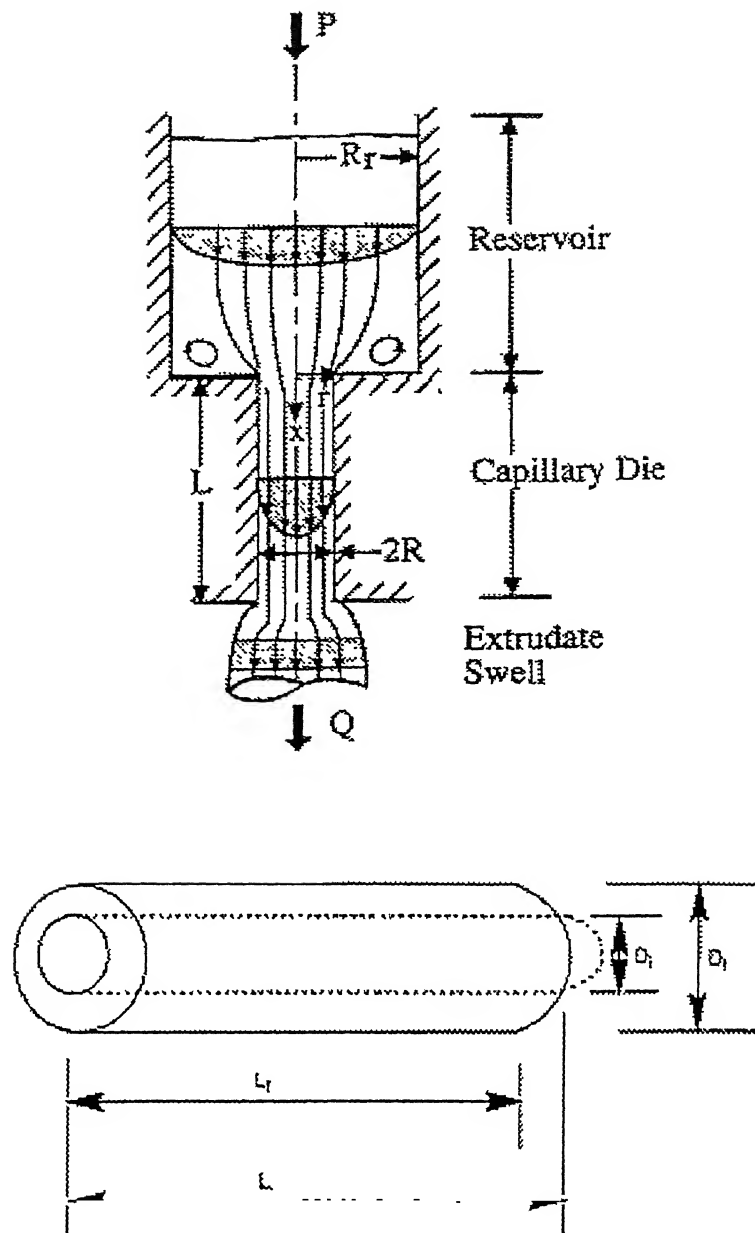
Fig. 1.1 Die Swell

1.1 Die Swell: Elastic Stress Relaxation Phenomenon

This seems to be general agreement that die swell is an elastic stress relaxation phenomenon. However, no single theory of die swell is accepted. Each theory is based on some assumptions regarding the effect of stress relaxation on the dynamics of the extrudate. A complication lies in the appearance of the recoverable shear strain S_R, which is defined as

$$S_R = \frac{\tau_{11} - \tau_{22}}{2\tau_{12}} \qquad\qquad ....(1.2)$$

where S_R, τ_{11}, τ_{22} and τ_{12} are the recoverable shear strain, first normal stress difference, second normal stress difference and shear stress respectively. This ratio of the primary normal stress difference to the shear stress (S_R), the stresses being calculated at the same shear rate in a steady simple shear flow, is not always available to accompany die swell data. Consequently the comparison of a die swell theory to experimental data often involves an uncertainty in the value of S_R itself [3].

1.2 Die Swell: Macroscopic Mass and Momentum Balance Approach

The solution of the die swell problem can be found by using macroscopic mass and momentum balance approach over a control volume bound by the capillary exit plane and another at a downstream position, where the velocity profile is in steady state [4]. This method has been successfully applied to the solution of die swell in Newtonian fluids. The results obtained by such balances in polymer do not agree with experimental data. A detailed study of extrudate swell analysis by macroscopic balance approach has been done by Bird et al. [5]. They [5] have distinguished the problem between two regimes: a low Reynolds number regime and a high Reynolds number regime. In the latter regime, a good agreement is observed by using only macroscopic mass and

3

momentum balance approach. But in the former regime the macroscopic mechanical energy balance has to be included in the analysis to get best results because of the significant effect of the viscous dissipation term. This renders the analysis more complicated as it requires detailed knowledge of the distorted surface, the distance between downstream to the fully developed flow, the velocity rearrangement in side the die, the Reynolds number and a new dimensionless group including the primary normal stress difference function ψ_1. Whipple's [6] careful experimental study of the velocity profile in the region before and after capillary exit is an initial step answering some of these needs. He has found that polymer melts "anticipate" the swelling phenomenon just after the exit point of die through decelerations and accelerations components of axial and radial velocity components. Thus the exit velocity profile is not the same as in the fully developed region.

1.3 Die Swell: Viscoelastic Fluid Theory Approach

Viscoelastic fluid theory approach is an important phenomenon to develop theoretical equations for prediction of die swell or to correlate with other rheological properties. Graessley et al. [7], Bagley and Duffy [8] and Funatsu and Mori [9] have considered an effective elastic body concepts to predict the die swell phenomenon. But Tanner [10] has considered an elastic recovery phenomenon to balance the stresses developed at the exit point of die. However more general correlations have been established based on the viscoelastic fluid theory by White and Roman [11], Huang and White [12] and Racin and Bogue [13]. They have related die swell with the normal stress to the shear stress ratio at the die wall. Quantitative experimental studies of the magnitude of extrudate swell have been reported by various investigators for long capillary [12-16] and for short capillary [17-18].

4

1.4 Die Swell: Finite Element Method Modeling and Finite Difference Modeling

Numerical methods such as finite element and finite difference methods are also used to predict die swell since 1974 [19-21] Most of works on die swell have been carried out mainly for isothermal systems There are few studies of non-isothermal die swell using finite element method Phouc and Tanner [22] have studied the effect of viscous heating on the swelling of extrudate But the effect of temperature-dependent physical properties on extrudate swell have been studies by Ben-Sabar and Caswell [23] and Nguyen and Boger [24] However McClelland and Finlayson [25] have calculated extrudate swell under both adiabatic and isothermal conditions through finite element method Reddy and Tanner [26] and Chang et al [27] have studied slit and circular geometries based on the collocation and Galerkin method, which is an extension form of classical displacement finite element method (or u-v-p) Crochet and Keunings [28] and Coleman [29] have obtained the results on slit die swell by using a mixed finite element method For Maxwell fluids, Bush et al [30] have presented planar and axisymmetric extrusion flow analysis using both finite element and boundary integral methods Limits of Deboarh number (De) for the finite element implementation is 1 5 The boundary integral formulation has produced a lower De limit of 0 75 for the fine mesh employed Subsequently, Bush [31] has made a detailed study on circular free-jet swelling behaviour for an Oldroyd-B model with varying polymer concentration

Experimental studies indicates that the non-elastic fluids at low Reynolds number exhibits a die swell, B of about 1.12 [32] But for high Reynolds number the value of B is about 0 87 There is a smooth transition between these two extreme limits [32] The effect of Reynolds number on the die swell has been observed by Metzner et al [4], they have found that at high Reynolds

number die swell is highly influenced by momentum fluxes and normal stresses but at low Reynolds number it is determined by rheological parameters through neglecting momentum fluxes

1.5 Factors Affecting Die Swell:

Die swell is a complicated function of few parameters, like die geometries; radius, length and entry angle, flow kinetics, the average flow rate and inertial effects, temperatures, die wall temperature, melt temperature, ambient temperature, heat transfer coefficient and specific heat, stresses developed, first normal stress difference and shear stress, molecular weight, molecular weight of melt and its distribution, and shear rate, etc So it is represented as

$$B = f\left(\gamma_w, \tau_w, L/D, T, t, MWD, \theta\right) \tag{1 3}$$

where B, γ_w, τ_w, L, D, T, t, MWD and θ are the die swell, wall shear rate, wall shear stress, length of the die, diameter of the die, melt temperature, residence time of melt in the die, molecular weight distribution and the die entrance angle respectively

1.5.1 Die Swell: Effect of Length to Diameter Ratio of Die (L/D)

Tadmor and Gogos [33] have reported that the die swell at constant wall shear stress decreases exponentially with increasing L/D up to 20, and then gradually becomes constant It is related to the ability of polymer melts and solutions to undergo delayed elastic strain recovery [33] The more strained and/or the more entangled melt gives more die swell From this point of view, the decrease of swelling with increasing L/D is due to two reasons First, in a long capillary the melt recovers from the tensile deformation suffered at the capillary inlet, which is due to the axial acceleration in that region Second, during shear flow the entanglement density is reduced, and so the ability of the

6

fluid to undergo strain recovery is also reduce Thus die swell at very large *L/D* value reflects the ability of the viscoelastic liquid to recover from shear strains only But for very short capillary, the large first normal stress difference that accompany the acceleration of the fluid through the entrance region of the capillary does not have sufficient time to relax and the first normal stress difference at the exit is considerably higher Therefore the melt coming from a very short capillary is much more entangled and recovers from both shear and tensile strains A representative curve for the effect of *L/D* ratio on die swell for low density polyethylene is shown in Fig 1 2 [1]
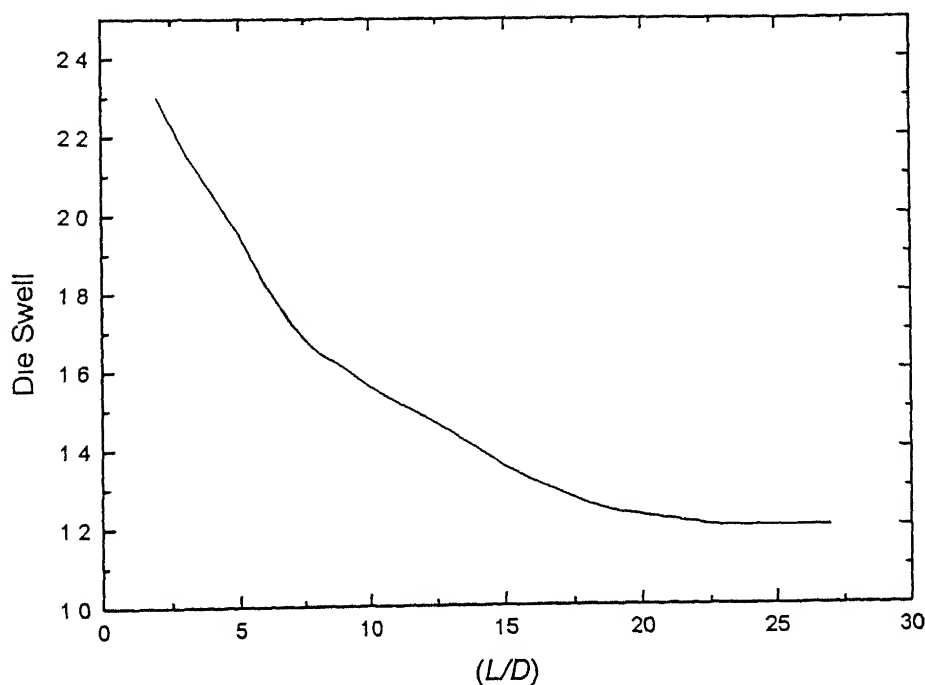
Fig. 1.2 *Die swell versus length/diameter for low density polyethylene (L is length of die and D is diameter of die)*

1.5.2 Die Swell: Effect of Shear Rate

The die swell for Newtonian fluids varies from 1 12 at low shear rates to 0 87 at high shear rates Similarly polymer melt exhibits the same value of die swell at lower shear rates in the Newtonian plateau region, but it is always greater than one (sometimes 200-500%) at high shear rates This is due to the decrease of viscosity with shear rate Fig 1 3 shows the effect of shear rate on die swell for polystyrene melt [33]
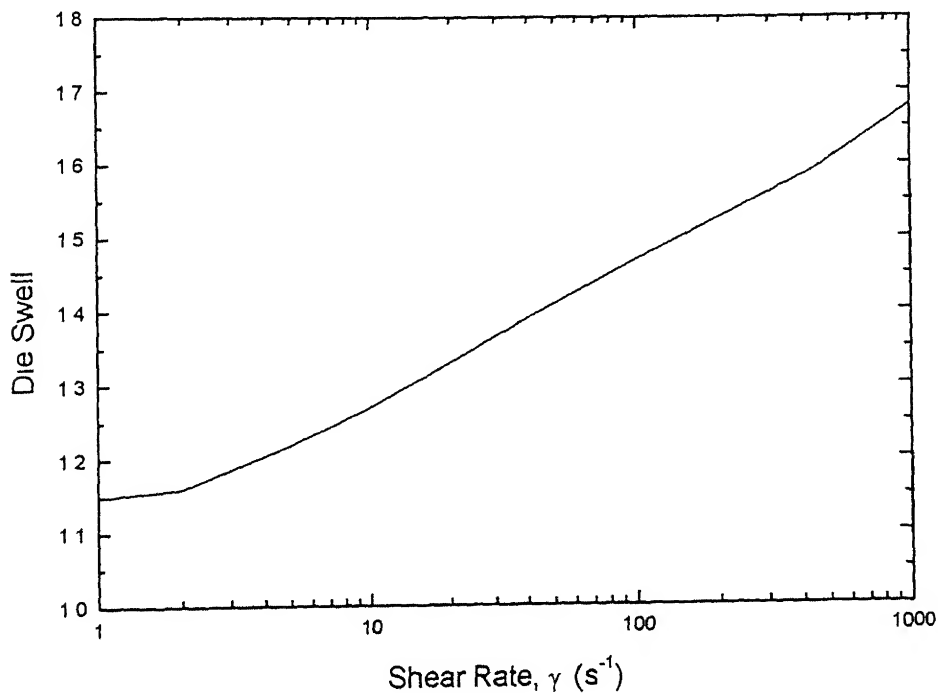
Fig. 1.3 *Effect of shear rate on die swell for polystyrene*

1.5.3 Die Swell: Effect of Shear Stress

Shear stress at the wall (τ_w) is a flow parameter which does not directly affect the die swell, but the first normal stress difference (N_1), which measures the extra tension during flow reflects the magnitude of die swell This is shown in Fig 1 4 for polystyrene the ratio of first normal stress difference to the shear stress causes an increase of the die swell in this figure This causes an increase in die swell Here the wall shear stress is defined as the pressure drop across the die without considering end effects divided by the suitable geometrical parameters For capillary dies, this is given by [34]

$$\tau_w = \frac{\Delta PR}{2L} \qquad (1\ 4)$$

where τ_w, ΔP, R and L are the average wall shear stress, pressure drop across the die, radius of the die and the length of the die respectively
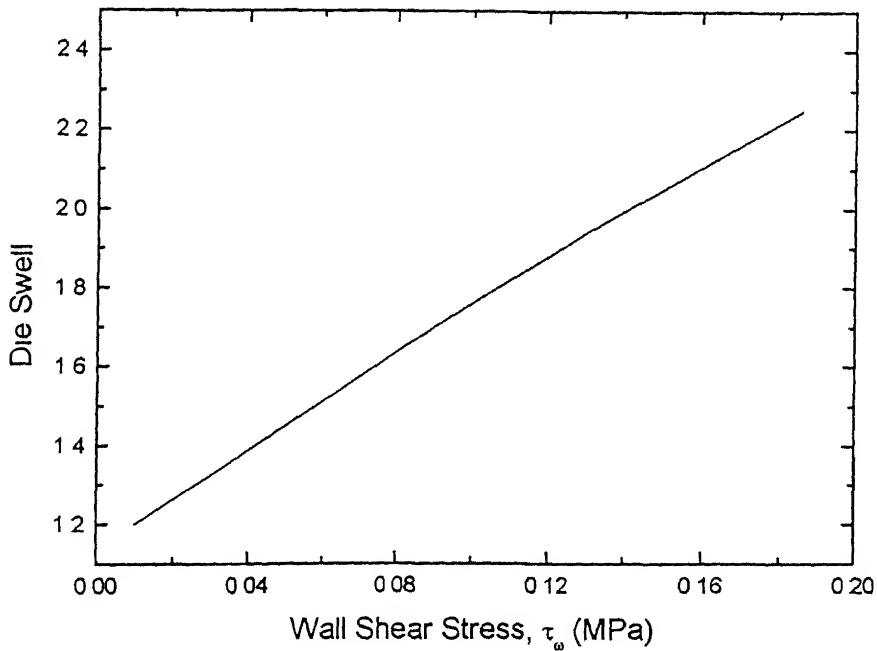
Fig. 1.4 *Die swell versus wall shear stress for polystyrene*

9

1.5.4 Die Swell: Effect of Temperature

Die swell depends on temperature In general as temperature of die wall and melt temperature increases, die swell decreases It also depends on flow rate, higher flow rates at low temperature usually result in a higher die swell for a given polymer melt Fig 1 5 shows annealed die swell versus flow under isothermal condition for polystyrene, where extrudate swell increases with an increase of flow rate but it decreases with increasing temperature [34] Under isothermal condition, die swell and first normal stress difference versus wall shear stress show a little dependence on temperature [35-36] But for polystyrene under isothermal condition, die swell against the average wall shear stress gives a temperature independent correlation However in non-isothermal condition, such a correlation is not exist [34]
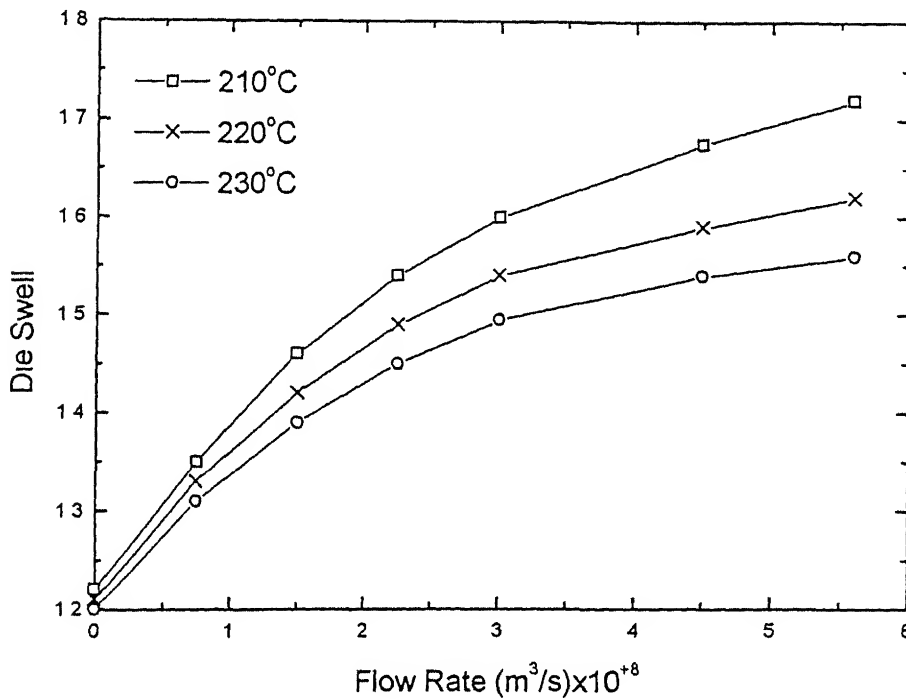
Fig. 1.5 *Die swell versus flow rate at different temperatures for polystyrene*

1.5.5 Die Swell: Effect of Molecular Weight and Its Distribution

The effect of molecular weight on die swell is complicated and not fully understood Effect varies from material to material and from linear to nonlinear dependency While it has been generally accepted that the increasing the molecular weight (M_w) and its distribution (MWD) of polymer melt at constant flow rate increases the die swell But no simple generalizations about the effect of molecular weight could be made This is true for most of the cases But large differences occur with an appreciable low-molecular-weight component, these small molecules seem to "lubricate" the swelling process and allow the "potential" die swell stored by the larger molecules to show itself It is understand that the narrow MWD samples show a delayed onset of elastic die swell (that is, a delayed departure from the low shear asymptote) and a steep slope once die wall begins compared with the broader distributions The effect of molecular weight (M_w) and molecular weight distribution (MWD) have been studied by several groups Mendelson and Finger [37], Shroff and Shida [38] and Shida et al [39] They have found that die swell increases with an increase of M_w and with broadening of MWD and vice versa for polystyrene But Mendelson and Finger [37] and Shroff and Shida [38] have presented opposite results for high density polyethylene (HDPE), where the die swell decreases with increasing M_w, although there is still a tendency to increase die swell when the distribution is broadened

1.5.6 Die Swell: Effect of Die geometry and Its Shape

Laun and Schuch [40] have reported the decrease of die swell with a decrease of die entry angle During converging flow, the polymer flow element is strongly stretched at the entry, but the effect is gradually decreases by the relaxation process, which proceeds within the capillary If the melt is sufficient elastic at the die exit it still remains some "memory" of the stretch given at the die entry, then at the exit of the die extrudate will swell in diameter The swell from slit dies is greater than that for capillaries [12] It may be due to the fact that in the slit die the relaxation phenomenon can't occur because of very short length, while in case of capillary it may occur because length is sufficient In case of capillary dies, the extrudate is straight and smooth at low shear rates When the shear rate is increased, a gross distortion set on at a certain value This gross distortion is preceded by surface roughness in some cases The form of distortion is different from polymer to polymer The polypropylene and polystyrene exhibits a characteristic waviness and a tendency to form spirals The low density polyethylene (LDPE) extrudates are distorted by the appearance of the knobby kinks at more or less regular intervals The high density polyethylene (HDPE) extrudates exhibited a pronounced waviness [41]

1.6 Measurement of Die Swell:

The die swell phenomenon encountered in the extrusion of viscoelastic materials is believed to elastic deformation incurred while the material flows through the extrusion apparatus [42-43] Previously there are two approaches to measure the die swell of polymer melts in the first approach, the melt is extrudate into a cool environment and then annealed to release stresses developed during extrusion, in the second approach, the melt is extrudate into a heated chamber or environment consisting either air or liquid [11,16], and then melt is allowed to swell in place But these two methods give different results Generally the isothermal environment method gives higher die swell than the annealing method [11] These two methods demand for the correction of the form [44]

$$\frac{d}{d_0} = \left(\frac{\rho_0}{\rho}\right)^{1/3} \qquad (1\ 5)$$

where d, d_0, ρ_0 and ρ are the swelled diameter of melt at extrusion temperature, swelled diameter of frozen polymer, density of frozen polymer and density of melt respectively The use of the density correction is questionable This is particularly true in the case of polymers, which crystallizes at the operating temperature In order to eliminate this source of possible error, the recent technique known as *"photographic technique"* given by Han and Charles [44] has been developed In this procedure, at first the polymer flows through a capillary device into a chamber, which is maintained at the same temperature as the capillary The chamber is equipped with a small removable *"pyrex"* window When a steady state is achieved, the window is removed and the polymer stream (still flowing) is cut at the exit The flow continues until a stream of about 3 in in length is emerged At this point flow is stopped and the small window is replaced This is accomplished by simply stopping the

13

extruder The pictures have to be taken from the suspended stream at various time intervals until the melt is fully relaxed Now the melt diameter can be determined by comparison of the melt images of standard samples

1.7 Previous Models: Quantification of Die Swell

Spencer and Dillon Model (1948): Spencer and Dillon [34] have proposed a relation between die swell and recoverable shear strain as

$$S_R = B^2 - B^{-2} \tag{1 6}$$

where S_R and B are the recoverable shear strain and die swell respectively

Nakajima and Shida Model (1966): Nakajima and Shida [45] have assumed that the overall bulk swelling is comparable to the instantaneous recovery of material elasticity from an imposed strain, which is related to flow condition in the die, and proposed a relationship between die swell and recoverable shear strain as

$$S_R = B^2 - B^{-4} \tag{1 7}$$

where S_R and B are the recoverable shear strain and die swell respectively

Tanner Model (1970) : An elastic-fluid theory of die swell for long dies has been presented by Tanner [12] This theory predicts that the die swell is asymptotically proportional to the cube root of the recoverable shear strain evaluated at the die wall The recoverable shear is defined as the ratio of first normal stress difference to the shear stress

$$B = \left[1 + \frac{1}{2} \left(\frac{N_1}{2\tau_w} \right)^2 \right]^{\frac{1}{6}} + 0\ 13 \tag{1 8}$$

where N_1, τ_w and B are the first normal stress difference, wall shear stress and die swell respectively This theory can not predict the die swell unless N_1 and τ_w are known for a given material

15

Bagley and Duffy Model (1970): Bagley and Duffy [8] have presented the theory of die swell by using constant strain energy function and a simplified relationship, which is obtained from the recoverable shear strain imposed on a flowing melt during capillary flow and the magnitude of the die swell emerging from the capillary This relates the average recoverable shear strain to the square of the die swell and is represented by

$$S_R = B^4 - B^{-2} \qquad (1\ 9)$$

where S_R and B are recoverable shear strain and the die swell respectively Here an end correction factor is needed to determine the recoverable shear strain at the die [46-47] and independent measurements of S_R and B are to be made

Mendelson and Finger Model (1971): Mendelson and Finger [48] have proposed a relationship between die swell and recoverable shear strain, given by

$$S_R^2 = B^2 \ln B \qquad ..\ (1\ 10)$$

where S_R and B are the recoverable shear strain and die swell respectively

Vlachopoulos Model (1972): Vlachopoulos [49] has proposed a relationship between die swell and recoverable shear strain, given by

$$S_R^2 = 3\left(B^4 + 2B - 3\right) \qquad (1\ 11)$$

where S_R and B are the recoverable shear strain and die swell respectively

White and Roman Model (1976): White and Roman [11] have analyzed the extrudate die swell problem in terms of the partially constrained elastic recovery theory based on Tanner's theory Here die swell is asymptotically

proportional to the cube root of the recoverable shear strain evaluated at the die wall and is represented as

$$B = C + \left[1 + \frac{1}{2} \left(\frac{N_1}{2\tau_w} \right)^2 \right]^{\frac{1}{6}}$$

(1 12)

where N_1, τ_w, B and C are first normal stress difference, wall shear stress, die swell and a material constant respectively

Vlcek model (1982): Vlcek [50] has proposed a relation between die swell, wall shear stress and the elastic modulus, given by

$$B^4 - B^{-2} = \frac{1}{2} \frac{\sigma_w}{G}$$

(1 13)

where B, σ_w and G are the die swell, wall shear stress and elastic modulus respectively

Macosko Model (1990): Macosko [51] has proposed a model based on maximum recoverable shear strain, which relates die swell to the square root of recoverable shear strain at the wall This is given by

$$B = \left[1 + \frac{1}{3} \left(\frac{N_1}{2\tau_w} \right)^2 \right]^{\frac{1}{4}} + 0\ 19$$

. (1 14)

where N_1, τ_w and B are first normal stress difference, wall shear stress and die swell respectively

Kumar Bhowmick and Gupta Model (1992): Kumar et al [52] have proposed a linear relationship between die swell and the maximum recoverable shear strain as

17

$$\alpha = 0.13\frac{N_1}{\tau} + 0.96 \qquad (1.15)$$

where α, N_1 and τ are the die swell, first normal stress difference and shear stress respectively. If N_1 is negative or the ratio of first normal stress to the shear stress is low, it predicts die swell less than one, which is not true for the case of general polymer (only liquid crystal polymer shows negative die swell)

1.8 Objective of the Present Work: -

It is recognized that die swell during polymer processing is not an intrinsic material property It depends on physical properties of the polymer, the physical and chemical properties of the compounding ingredients and their interaction with polymer and operating variables Therefore, a reliable relationship for the prediction of die swell is desirable to obtain a better understanding of die swell phenomenon The existing models described earlier are mostly based on the processing behaviour of a polymer melt in a capillary rheometer But the flow field in actual processing condition is known to be different from that in the capillary rheometer Therefore, to get accurate data during processing of a polymeric material, Randcastle microtruder (Model no RCO625) is used here A survey of the literature alerts us to several unanswered questions on die swell These questions include

1) Are the Tanner's model (1970) [12], Bagley's model (1970) [8], White and Roman's model (1976) [11], Macosko's model (1990) [51] and Kumar et al model (1992) [52] applicable to all polymer or to a specific polymer?

2) Is Macosko's model (1990) [51] applicable to a capillary geometry?

3) Do the Tanner's model (1970) [12], Bagley's model (1970) [8], White and Roman's model (1976) [11], Macosko's model (1990) [51] and Kumar et al model (1992) [52] depend on the processing temperature, shear rate, length to diameter ratio of the die and compounding ingredients present in the polymer?

4) If the coefficients and constants in the above models are not constant then how do they vary with the above variables?

5) Is it possible to correlate the coefficients and adjustable constants of the above models?

6) Does die swell depend on the basic polymer material properties like Young's modulus, storage modulus, loss modulus, viscosity, etc ?

7) Is it possible to calculate maximum recoverable deformation from the Tanner's model (1970) [12], Bagley's model (1970) [8], White and Roman's model (1976) [11] and Macosko's model (1990) [51]?

8) How does the maximum recoverable deformation calculated from the Tanner's model (1970) [12], Bagley's model (1970) [8], White and Roman's model (1976) [11] and Macosko's model (1990) [51] vary from other models i e Kumar et al model (1992) [52]?

9) What is the degree of dependence of die swell on maximum recoverable shear deformation?

The present investigation, after a theoretical overview, will attempt to address some of these unsolved problems and to explain the die swell behaviour of low density polyethylene, polypropylene and polystyrene over a wide range of shear rates, temperatures, average velocity of flow and radius of die Further more, development of a quantitative model equation for predicting die swell from the maximum recoverable deformation, shear rate, relaxation time, average velocity of flow and radius of die based on elastic recovery theory is to be made

CHAPTER 2
EXPERIMENTAL

2.1 Materials:

Low density polyethylene, polypropylene and polystyrene both amorphous and crystalline were used in this investigation and supplied by Huntsman Chemical Corporation, USA The specifications of low density polyethylene, polypropylene and polystyrene (both amorphous and crystalline) are given in Tables 2 1-2 3 respectively.

Table 2.1: Specifications of low density polyethylene (LDPE) [53]

PROPERTIES	A S T M TEST NO	LDPE
Melting point, $^\circ$C	-	125
Glass transition temperature, $^\circ$C	-	-30
Compression ratio	-	1 80-3 60
Specific gravity	D792	0 91-0 92
Specific vol , 10^{-3} m^3/kg	D792	1 10
Refractive index, n	D542	1 51
Tensile strength, MPa	D638	6 80-15 60
Elongation, %	D638	90 00-800 00
Tensile modulus, MPa	D638	115 60-238 00
Hardness (Shore D)	D785	41-46
Thermal conductivity, 10^{-4} cal /sec /cm^2	C177	8 00
Specific heat, cal/$^\circ$C/gm	-	0 55
Resistance to heat, $^\circ$C	-	82 00-100 00
Thermal expansion, 10^{-5} per $^\circ$C	D696	16 01-18 00
Dielectric constant, 10^6 cycles	D150	2 30-2 40
Dissipation factor, 10^6 cycles	D150	<0 0005

Table 2.2: Specifications of Polypropylene [54]

PROPERTIES	A S T M TEST NO	POLYPROPYLENE
Melting point, °C	-	138
Glass transition temperature, °C	-	-80
Compression ratio	-	2 00-2 40
Specific gravity	D792	0 90-0 91
Specific vol , 10^{-3} m^3/kg	D792	1 10
Refractive index, n	D542	1 50
Tensile strength, MPa	D638	29 20-37 40
Elongation, %	D638	200 00-700 00
Tensile modulus, MPa	D638	1088 00-1530 00
Comp Strength, MPa	D695	37 40-54 40
Hardness (Shore D)	D785	85 00-110 00
Thermal conductivity, 10^{-4} cal /sec /cm^2	C177	2 80
Specific heat, cal/°C/gm	-	0 50
Thermal expansion, 10^{-5} per °C	D696	5 80-10 20
Resistance to heat, °C	-	121 00-160 00
Dielectric constant, 10^6 cycles	D150	2 20-2 60
Dissipation (power) factor, 10^6 cycles	D150	<0 0005-0 002

Table 2.3: Specifications of Polystyrene

PROPERTIES	A S T M TEST N0	AMORPHOUS [55]	CRYSTA-LLINE WA552 [56]
Melting point, °C	-	240	263
Glass transition temperature, °C	-	-80	-100
Compression ratio	-	1 60-2 30	-
Specific gravity	D792	1 04-1 09	1 24
Specific vol ,10^{-3} m^3/kg	D792	0 95	-
Refractive index, n	D542	1 60	-
Tensile strength, MPa	D638	34 00-81 60	105 00
Elongation, %	D638	1 00-2 50	2 20
Tensile modulus, MPa	D638	2720 00-4080 00	7580 00
Comp Strength, MPa	D695	78 20-108 80	-
Hardness (Shore D)	D785	M65-M80	-
Thermal conductivity, 10^{-4} cal /sec /cm^2	C177	2 40-3 30	-
Specific heat, cal/°C/gm	-	0 32	-
Thermal expansion, 10^{-5} per °C	D696	6 80	1 90
Resistance to heat, °C	-	66 01-77 05	-
Dielectric constant, 10^6 cycles	D150	2 40-2 70	3 10
Dissipation (power) factor, 10^6 cycles	D150	0 0001-0 0004	0 001

2.2 Die Swell:

The extrudates coming out from the capillary of the Randcastle microtruder were collected for the measurement of equilibrium die swell, taking maximum care to avoid any further deformation The diameter of the extrudate was measured after equilibrium was reached For measuring the diameter of an extrudate, a fixed length of the uniform portion of the extrudate was cut, and its weight was taken, as accurately as possible The diameter of the extrudate was then calculated by the following relations

$$Volume \ of \ the \ extrudate \ (V_e) = \frac{\pi D_e^2 l_e}{4} \qquad (2\ 1)$$

$$Density \ (\rho) = \frac{M}{V_e} = \frac{M}{\pi D_e^2 l_e / 4} \qquad (2\ 2)$$

$$Diameter \ of \ the \ extrudate \ (D_e) = \left(\frac{4M}{\pi l_e \rho}\right)^{1/2} \qquad .(2\ 3)$$

where l_e, M and D_e are the measurable quantities for the length, mass and diameter of the extrudate respectively

The equilibrium die swell at room temperature is then calculated by using the following relation

$$Equilibrium \ die \ swell \ (\alpha) = dia \ of \ extrudate/dia \ of \ the \ capillary \qquad (2\ 4)$$

The die swell at the experimental temperature is obtained from the relation

$$\alpha = die \ swell \ at \ room \ temperature + \beta \qquad (2\ 5)$$

where β is the volume expansion coefficient of the material.

Apparent wall shear rate $\left(\gamma_{W,a}\right)$, wall shear rate $\left(\gamma_W\right)$, shear stress $\left(\tau_W\right)$ and pressure difference (ΔP) across the length of the capillary in the Randcastle microtruder is obtained from the following equations

$$\gamma_{W,a} = \frac{32 Q_P}{\pi d_c^3} \tag{2 6}$$

$$\gamma_W = \frac{3n+1}{4n}\gamma_{W,a} \tag{2 7}$$

$$\tau_W = \eta \gamma_W \tag{2 8}$$

$$\Delta P = \frac{4\tau_W l_c}{d_d} \tag{2 9}$$

where Q_P, d_c, n, η and l_c are the volumetric flow rate, diameter of the die, non-Newtonian flow index, viscosity obtained from the advanced rheometric expansion system (ARES) instrument under steady shear condition using parallel plate-plate configuration and the length of the die respectively

These die swell experiments were performed in Randcastle microtruder (Model no RO625) The measurements of die swell through an extruder as a function of rotor speed, L, D_t (length/diameter) of the capillary die and temperature were carried out for low density polyethylene, polypropylene and polystyrene (both amorphous and crystalline grades) over a range of temperature (150 to 290°C), rotor speed (5 to 30 rpm) and two different $L_t D_t$

ratio of die (82/2 5 and 62/8) Experimental results were reproducible within $\pm 5\%$ error

The values of volume expansion coefficient (β) used in above equation were taken from the literature (Brandrup and Immergut, 1989 [57])

2.3 Rheological Properties:

Rheological properties of low density polyethylene, polypropylene and polystyrene both amorphous and crystalline grades were measured by Advanced Rheometric Expansion System Spectrometer in a parallel plate-plate configuration Experimental studies were carried out in steady shear condition over a range of temperature from 150 to 290°C and shear rate from 0 01 to 400 s^{-1} following standard methods (Macosko 1990 [51], Collyer and Clegg 1998 [58]) Experimental results were reproducible within $\pm 5\%$ error.

CHAPTER 3
PROPOSED MODEL

The melt elasticity of polymeric materials in shearing flow through a die manifests itself at the die exit in the form of an expansion of cross-sectional area of the extrudate to a size greater than that of the die. This causes extrudate diameter of large dimension than the diameter of die, called as die swell [59], memory [47], puff-up [37] Barus-effect [47], etc. This phenomenon is common in the possessing of polymers. And also non-elastic fluids emerge from a capillary with a diameter different from that of the die diameter. Experimental studies for such non-elastic liquids at low Reynolds number indicate that the emergent stream exhibits a die swell, B of about 1.12. However at high Reynolds number the emergent stream contracts giving a value of die swell of about 0.87 [32]. Common example is liquid crystal polymers. However this effect is small compared with the viscoelastic polymeric melts.

It is generally agreed that, this swelling ratio is strongly dependent on the first normal stress difference [3], shear stress [34], length/diameter ($L D$) of die [33] and shear rate [33] in the die, etc. It decreases rapidly with increasing L/D up to 20, and then gradually becomes constant [60]. It increases with shear rate [33] and die wall shear stress [34]. This is due to elastic recovery of the material.

At high extrusion rates, distortion occurs. This has a form of helical extrudate in the melt emerging from the circular dies [12] and provides the limit for maximum shear rate. In general this expansion occurs in two steps: the first is very rapid, relatively larger in magnitude and close to the die exit, and the secondary expansion occurs slowly much smaller in magnitude and far away from the die.

Lodge [61] has shown theoretically how a sheared piece of material exhibits elastic recovery and swelling when it is released from stress instantaneously and how a small, slow and further recovery takes place [62]. During the last five decades, mathematical constitutive theories for non-linear large elastic deformation of viscoelastic materials have been developed on the basis of statistical mechanics and strain energy density function. However, quantitative evaluation of die swell is not easy. Early attempts of deriving mathematical expression are not successful due to the complexities of mathematical formulations and the lack of general guidelines. Since the extrudate swell is helpful to understand the design parameters during mould design of a polymeric product, an effort is made here to quantify it. The elastic energy stored in a polymeric material during flow through a die is proportional to the first normal stress difference, shear stress applied to the material and its maximum recoverable deformation. Based on these facts the first normal stress difference, shear stress, shear rate, time-temperature superposition principle and die geometry are considered here to develop a new model.

Now to proposed a new model for quantification of die swell, the following assumptions are made.

1) The slow recovery of die swell far away from the die is ignored.

2) Second normal stress difference is very small in magnitude compared with first normal stress difference.

3) Inertial effects in the flow are ignored.

4) Gravity, other body forces, surface tension forces are ignored, so that the final extrudate is load free.

3.1 Effect of First Normal Stress Difference and Shear Stress:

Let a fluid characteristic time (θ) is large compared with the mean time taken to clear the exit zone of a die having diameter d, than most of materials make a fast change from the state of fully developed flow into a state of zero stress measured relative to the atmospheric pressure as datum [10]. Then

$$u\theta/d \gg 1 \qquad \qquad \text{......(3.1)}$$

where u is the average velocity.

If inertia forces in the sample is completely neglected, then

$$\rho ud/\eta \ll 1 \qquad \qquad \text{.....(3.2)}$$

where η is a characteristic viscosity and ρ is the melt density. But it is noted that for a unit strain and modulus η/θ, the "elastic" stresses are much greater than inertia forces. This is represented as [10]

$$\rho u^2 \theta/\eta \ll 1 \qquad \qquad \text{...(3.3)}$$

Since material is flowing through the capillary where all the constraints are suddenly removed and the stresses are brought instantaneously to zero, it is assumed that K-BKZ (Kaye [63], Bernstein, Kearsley and Zapas [64]) form is relevant, which is given by

$$T = -p\partial_{ij} + \int_{-\infty}^{t} \left(\frac{\partial U}{\partial I_B} B - \frac{\partial U}{\partial I_C} C \right) dt' \qquad \qquad \text{.....(3.4)}$$

where U is a function of I_B, I_C and t-t'. $B (\equiv C^{-1})$ and C are the Finger and right Cauchy-Green strain tensors at time t' in the past measured relative to the configuration of the material at time t in the present respectively. I_B and I_C are the traces of B and C respectively. p is the hydrostatic pressure and δ_{ij} is the Kronecker delta.

The velocity field in a simple shearing flow is represented as [65].

$$V = (\gamma y, 0, 0) \qquad \qquad \text{......(3.5)}$$

$$x = X + \gamma Y, \; y = Y \text{ and } z = Z \qquad \cdots (3.6)$$

then,

$$T + p\partial_y = \begin{bmatrix} S_{xx} & S_{xy} & 0 \\ S_{yx} & S_{yy} & 0 \\ 0 & 0 & 0 \end{bmatrix} \qquad \cdots (3.7)$$

where

$$S_{xx} - S_{yy} = N_1 \left(\gamma \right) = \int_0^\infty \left(\frac{\partial U}{\partial I_B} + \frac{\partial U}{\partial I_C} \right) \gamma^2 s^2 ds \qquad \cdots (3.8)$$

$$S_{yy} - S_{zz} = N_2 \left(\gamma \right) = \int_0^\infty \left(\frac{\partial U}{\partial I_C} \right) \gamma^2 s^2 ds \qquad \cdots (3.9)$$

and

$$S_{xy} = S_{yx} = \tau \left(\gamma \right) = \int_0^\infty \left(\frac{\partial U}{\partial I_B} + \frac{\partial U}{\partial I_C} \right) \gamma \, s ds \qquad \cdots (3.10)$$

But for the sake of simplicity, N_2 is neglected here [$N_2 \ll N_1$, based on the experimental observation].

Let the viscometric history up to a time just less than zero, then a sudden strain jump occurs. If present calculation applies to the instant just after the strain jump then in the previous equation (3.4), it is necessary to find out B and C

$$B = C^{-1} = (F^T F)^{-1} \qquad \cdots (3.11)$$

where F is relative deformation gradient. Let the material which is at the spatial coordinate X at the time t is at the position r at the time t', then F is defined as

$$F = \delta r / \delta x. \qquad \cdots (3.12)$$

The strain at the sudden jump may be written in terms of deformation gradient F_o, from the chain rule of differentiation [66]

$$F = F^{(v)} F_o \qquad \ldots(3.13)$$

where $F^{(v)}$ is a viscometric history gradient. $F^{(v)}$ and F_o at time t' are represented by

$$F^{(v)} = \delta r / \delta x' \qquad \ldots(3.14)$$

$$F_o = \delta x' / \delta x \qquad \ldots(3.15)$$

where x' is a reference point.

From equation (3.13), this $F^{(v)}$ is also represented in polar coordinates (z', r', θ')

$$F^{(v)} = \begin{bmatrix} 1 & -\gamma s & 0 \\ 0 & 1 & 0 \\ 0 & 0 & 1 \end{bmatrix} \qquad \ldots(3.16)$$

where the velocity is $[u(r'), 0, 0]$, $s = t - t'$ and $\gamma = \delta u / \delta r'$, the local shear rate.

Now it is considered that the material at a time t is just greater than zero. Then in equation (3.4), T is 0 but p is unknown. Now to find unknown parameter equations (3.4), (3.11) and (3.13) give

$$p F_o F_o^T = \int_0^\infty U'(tr F_o^{-1} B^{(v)} (F_o^T)^{-1}, s) B^{(v)}(s) ds \qquad \ldots(3.17)$$

where $U' = \delta U / \delta I_B$, p is an unknown pressure, and

$$B^{(v)} = \begin{bmatrix} 1 + \gamma^2 s^2 & \gamma s & 0 \\ \gamma s & 1 & 0 \\ 0 & 0 & 1 \end{bmatrix} \qquad \ldots(3.18)$$

The solution of equation (3.17) for F_o is not feasible in general unless U' is known numerically. For this purpose it is assumed that U' is smooth enough to expand in a Taylor series with the difference of $tr\,B$ and $tr\,B^{(v)}$. Let

$$\Delta I_B = tr B - tr B^{(v)} = tr\left\{ F_o^{-1} B^{(v)} (F_o^T)^{-1} \right\} - 3 - \gamma^2 s^2 \qquad \ldots(3.19)$$

Expansion of U' in a series of I_B gives

$$U' = U'\ (3+\gamma^2 s^2, s) + (\delta U'/\delta I_B)\ \Delta I_B + 1/2(\delta^2 U'/\delta I_B^2)\ (\Delta I_B)^2 + \ldots \qquad ..(3.20)$$

Let

$$\gamma^n \int_0^\infty s^n U(3+\gamma^2 s^2, s)ds = G, \tau, N_1 \qquad ...(3.21)$$

where G is an elastic modulus, τ is the local shear stress in the capillary and N_1 is the corresponding first normal stress difference.

Let $F_o F_o{}^T$ is volume-preserving, set det F_o is equal to one in the equation (3.17) and after simplifying U' from equations (3.17) and (3.19), p is represented as

$$p^3 = G(G^2 + N_1 G - \tau^2) \qquad ....(3.22)$$

Now the strain field $F_o F_o{}^T$ should satisfy the compatibility conditions for finite strains. This gives

$$F_o F_o{}^T = p^{-1} \begin{bmatrix} G+N_1 & \tau & 0 \\ \tau & G & 0 \\ 0 & 0 & G \end{bmatrix} \qquad .....(3.23)$$

where $p = G(1+N_1/G-\tau^2 G^2)^{1/3}$. If the deformation gradient field is assumed to be independent of the axial coordinate z, the deformation for an incompressible solid rod is represented as

$$z' = (z/\lambda^2) + g(r) \qquad ....(3.24)$$

$$r' = \lambda r \qquad ....(3.25)$$

$$\theta' = \theta \qquad ...(3.26)$$

where λ is a constant. Here $\qquad g'=dg/dr \qquad ....(3.27)$

$$F_o = \begin{bmatrix} \dfrac{1}{\lambda^2} & g' & 0 \\ 0 & \lambda & 0 \\ 0 & 0 & \lambda \end{bmatrix} \qquad ....(3.28)$$

$$F_oF_o^T = \begin{bmatrix} \frac{1}{\lambda^4}+g'^2 & \lambda g' & 0 \\ \lambda g' & \lambda^2 & 0 \\ 0 & 0 & \lambda^2 \end{bmatrix} \qquad \text{....(3.29)}$$

But equations (3.27), (3.28) and (3.29) are not strictly compatible with equation (3.23) because G, N_1 and τ are independent parameters. To solve this problem it is assumed that all of the stress components are zero at the exit point (except τ_{zz}) then for a stress free extrudate

$$2\pi \int_0^{\frac{D}{2}} \tau_{zz} r dr = 0 \qquad \text{....(3.30)}$$

Now assuming a deformation gradient F_o of the form (3.27), (3.28) and (3.29) with relaxing the above condition and after repeating the analysis the final form of the stress-matrix is

$$P\lambda^2 = G \qquad \text{....(3.31)}$$

$$P\lambda g' = \tau \qquad \text{....(3.32)}$$

$$N_1 + G - (\tau_{zz}/\lambda^4) = p[(1/\lambda^4) + g'^2] \qquad \text{.....(3.33)}$$

Now eliminate p and g' from equation (3.33) by using equation (3.32), the first normal stress difference is represented as

$$N_1 + G - (\tau_{zz}/\lambda^4) = (G/\lambda^6) + (\tau^2/G) \qquad \text{...(3.34)}$$

Integrating equation (3.34) over the cross-section and using equation (3.30) gives an equation for the radial expansion $1/\lambda$ as

$$\frac{1}{\lambda} = \frac{D}{d} = \left\{ \frac{\displaystyle\int_0^{D/2}(N_1 + G - \tau^2/G)r dr}{\displaystyle\int_0^{D/2} G r dr} \right\}^{\frac{1}{6}} \qquad \text{.....(3.35)}$$

Here N_1, G and τ are variables. These are expressed in terms of r' and θ' because of the linear transformation $r' = \lambda r$.

Now taking $\xi = 2\,r'/d$ and integrating over the cross-section the following equations are obtained as

$$\overline{G} = 2\int_0^1 G(\xi)d\xi \qquad \qquad \text{......(3.36)}$$

$$\left(\frac{D}{d}\right)^6 = 2\int_0^1 \left(1 + \frac{N_1}{\overline{G}} - \frac{\tau^2}{\overline{G}^2}\right)\xi d\xi \qquad \qquad \text{.....(3.37)}$$

Now putting $N_1/2\tau = \tau/G = S_R$, where S_R is the maximum recoverable shear and integrating equation (3.37) gives

$$(B)^6 = \left(\frac{D}{d}\right)^6 = \left(1 + \frac{N_1^2}{4\tau^2}\right) \qquad \qquad \text{....(3.38)}$$

The equation (3.38) shows the effect of first normal stress difference and shear stress on the die swell.

3.2 Effect of Shear Rate:

To understand the effect of shear rate on die swell a single integral constitutive equation (3.39) is used here [67-68]

$$\sigma = -p\partial_{ij} + \int_0^\infty m_1(z)C_{ij}^{-1}dz \qquad \qquad ....(3.39)$$

where σ, p and δ_{ij} are the stress tensor, hydrostatic pressure and Kronecker delta respectively. C_{ij}^{-1} and $m_1(z)$ are expressed as

$$C_{ij}^{-1} = \frac{\partial x^i}{\partial x_a}\frac{\partial x^j}{\partial x_a} \qquad \qquad .....(3.40)$$

and

$$m_1(z) = \frac{G}{t_n^*}\exp\left(-\frac{z}{t_n^*}\right) \qquad \qquad .....(3.41)$$

This equation is a form of Maxwell relaxation function. x_i is the instantaneous position and x_a is the past configuration in cartesian coordinates.

Considering a flow for long duration and elongation in nature, the shear rates are represented as

$$\frac{dx_1}{dt} = \gamma_1 x_1 \qquad \text{and} \qquad \frac{dx_2}{dt} = \gamma_2 x_2 \qquad .....(3.42)$$

This leads to

$$x_1(t) = x_1(0)\int_e \gamma_1 \, ds \qquad \text{and} \qquad x_2(t) = x_2(0)\int_e \gamma_2 ds \qquad .....(3.43)$$

Now a matrix Q is introduced in equation (3.39) to simplify kinematic considerations. This gives

$$Q\left(\sigma_{ij} + p\partial_{ij}\right)Q^T = \int_0^\infty m_1(z)QC^{-1}Q^T dz \qquad .....(3.44)$$

For an elongation flow

$$QC^{-1}Q^T = \begin{bmatrix} \lambda_1^2 & 0 & 0 \\ 0 & \lambda_2^2 & 0 \\ 0 & 0 & 1 \end{bmatrix} \qquad \text{....(3.45)}$$

where $\quad \lambda_1 = \int \gamma_1 dz \quad$ and $\quad \lambda_2 = \int \gamma_2 dz \qquad$ ....(3.46)

But the die swells are represented as

$$x_1(t_r) = \frac{1}{\alpha_1} x_1(t) \qquad x_2(t_r) = \frac{1}{\alpha_2} x_2(t) \qquad x_3(t_r) = x_3(t) \qquad \text{....(3.47)}$$

Now the left hand side of equation (3.44) is written as

$$Q(\sigma_{ij} + p\partial_{ij})Q^T = \begin{bmatrix} \dfrac{1}{\alpha_1^2}(\sigma_{11} + p) & 0 & 0 \\ 0 & \dfrac{p}{\alpha_2^2} & 0 \\ 0 & 0 & p \end{bmatrix} \qquad \text{....(3.48)}$$

Equating equation (3.44) with equation (3.48), the die swells are obtained as

$$\frac{1}{\alpha_1^2}(\sigma_{11} + p) = \int_0^\infty \frac{G}{t_n^*} \exp\left(-\frac{z}{t_n^*}\right)\lambda_1^2 dz = I_1 \qquad \text{.... (3.49)}$$

$$\frac{p}{\alpha_2^2} = \int_0^\infty \frac{G}{t_n^*} \exp\left(-\frac{z}{t_n^*}\right)\lambda_2^2 dz = I_2 \qquad \text{....(3.50)}$$

Eliminating p from equation (3.49) by putting equation (3.50) leads to

$$\frac{1}{\alpha_1^2}\sigma_{11} + \frac{\alpha_2^2}{\alpha_1^2}I_2 = I_1 \qquad \text{..... (3.51)}$$

Now integrating across the cross-section and taking the integral of σ_{11} to be zero gives

$$\int_0^A \frac{\alpha_2^2}{\alpha_1^2} da = \frac{\displaystyle\int_0^A I_1 da}{\displaystyle\int_0^A I_2 da} = \frac{\displaystyle\int_0^A \int_0^\infty \exp-\left[\frac{z}{t_n^*} + 2\int \gamma_1 dz\right] dz da}{\displaystyle\int_0^A \int_0^\infty \exp-\left[\frac{z}{t_n^*} + 2\int \gamma_2 dz\right] dz da} \qquad \text{....(3.52)}$$

Taking kinematics to be independent of cross section and independent of time with

$$\int \gamma_j \, dz = X_{jz} \qquad (j = 1, 2) \qquad \qquad \text{....(3.53)}$$

Equation (3.52) gives

$$\int_0^A \frac{\alpha_2^2}{\alpha_1^2} da = \frac{1 - 2t_n^* X_2}{1 - 2t_n^* X_1} \qquad \qquad \text{....(3.54)}$$

For a capillary die [13]

$$\alpha_1 = \frac{1}{\alpha_2^2} \qquad \text{and} \qquad \int_0^A \frac{\alpha_2^2}{\alpha_1^2} da = B^6 \qquad \qquad \text{....(3.55)}$$

Since

$$\gamma_2 = -\frac{1}{2} \gamma_1 \qquad \qquad \text{....(3.56)}$$

Equations (3.54), (3.55) and (3.56) give

$$B^6 = \frac{1 + t_n^* \gamma_1}{1 - 2t_n^* \gamma_1} \qquad \qquad \text{....(3.57)}$$

3.3 Time-Temperature Superposition:

Extensive literature survey [69-72] indicates the dependency of die swell on temperature. To eliminate this parameter time-temperature superposition principle is applied here. The relaxation time (t_n^*) is a function of temperature (T). It is represented by the product of shift-factor (α_T) and the relaxation time (t_n) at a reference temperature. Generally glass transition (T_g) temperature is taken as a reference point.

This shift factor is represented by Williams, Landel and Ferry (WLF) equation [73]

$$\log \alpha_T = \frac{-c_1(T-T_g)}{c_2 + T - T_g} \quad \quad ....(3.58)$$

where T and T_g are the temperature and glass transition temperature respectively. c_1 and c_2 are constants.

A single integral constitutive equation "Time-Temperature Superposition" principle is adopted here

$$\sigma_{ij} = -p\partial_{ij} + \sum_n G_n \frac{T(t)}{T_o} \int_{-\infty}^{t} \frac{\exp-\left(\frac{t-t'}{t_n^*}\right)}{t_n^*} c_{ij}^{-1} dt' \quad \quad ....(3.59)$$

where σ_{ij}, p, δ_{ij}, G_n, t, t' and C_{ij}^{-1} are the stress tensor, pressure, Kronecker delta, elastic modulus, time in to consideration, past time and relative Finger strain tensor respectively.

Neglecting the modulus factor [74] [avoid complexity] equation (3.59) leads to

$$\sigma_{ij} = -p\partial_{ij} + G \int_{-\infty}^{t} \frac{\exp-\left(\frac{t-t'}{t_n^*}\right)}{t_n^*} c_{ij}^{-1} dt' \quad \quad ....(3.60)$$

where

$$t_n^* = \frac{t_n \alpha_T}{1 + b \Pi_d^{1/2} t_n \alpha_T}$$ ....(3.61)

where Π_d is the second invariant of the deformation rate and b is an empirical dimensionless parameter of order 0.5. Taking b is equal to zero [75], equation (3.61) gives

$$t_n^* = \alpha_T t_n$$ ....(3.62)

Now a Cartesian coordinate systems [1,2,3], which is translating with the material is assumed here. Within this frame the points are assigned using spatial coordinates $x'(t')$ at an arbitrary past time t' and the body coordinates $X'(t')$ at an arbitrary past time t'. This is represented by

$$x^1 = \lambda\,(X^1 + X^2\,\dot{\gamma}\,(r)\,t')$$ ....(3.63)

$$x^2 = \lambda^{-1/2}\,X^2$$ ....(3.64)

$$x^3 = \lambda^{-1/2}\,X^3$$ ...(3.65)

But λ is equal to one due to the incompressibility of material. This gives

$$C_{ij}^{-1} = \frac{\partial x^i}{\partial X_a}\frac{\partial x^j}{\partial X_a}$$ ....(3.66)

Now introducing a matrix Q and a transform matrix Q^T in the eq. (3.59)

$$Q(\sigma_{ij} + p\partial_{ij})Q^T = \frac{G}{t_n^*}\int_{-\infty}^{t}\exp-\left(\frac{t-t'}{t_n^*}\right)Qc_{ij}^{-1}Q^T dt'$$ ....(3.67)

with

$$Qc_{ij}^{-1}Q^T = \begin{bmatrix} 1+\dot{\gamma}^2\,t'^2 & \dot{\gamma}t' & 0 \\ \dot{\gamma}t' & 1 & 0 \\ 0 & 0 & 1 \end{bmatrix}$$ ....(3.68)

and introducing parabolic velocity distribution as

$$\gamma(r) = \left|\frac{dv(r)}{dr}\right| = \frac{4vr}{R^2} \qquad \text{....(3.69)}$$

Now the swell has the forms in polar coordinates as

$$x_1(t_r) = \frac{1}{\alpha_1}x_1(t) \qquad x_2(t_r) = \frac{1}{\alpha_2}x_2(t) \qquad x_3(t_r) = x_3(t) \qquad \text{.... (3.70)}$$

Introducing Q and Q^T in equation (3.67)

$$Q(\sigma_y + p\partial_y)Q^T = \begin{bmatrix} \frac{1}{\alpha_1^2}(\sigma_{11}+p) & 0 & 0 \\ 0 & \frac{p}{\alpha_2^2} & 0 \\ 0 & 0 & p \end{bmatrix} \qquad \text{....(3.71)}$$

Now putting $Qc_{ij}^{-1}Q^T$ in equation (3.67) and comparing with equation (3.71), the following equations are obtained as

$$\frac{1}{\alpha_1^2}(\sigma_{11}+p) = \frac{G}{t_n^*}\int_0^\infty \exp-\left(\frac{t-t'}{t_n^*}\right)\left(1+\gamma^2 t'^2\right)dt' = I_1 \qquad \text{....(3.72)}$$

and

$$\frac{p}{\alpha_2^2} = \frac{G}{t_n^*}\int_0^\infty \exp-\left(\frac{t-t'}{t_n^*}\right)dt' = I_2 \qquad \text{....(3.73)}$$

Eliminating p from equation (3.72) by equation (3.73) give

$$\frac{\sigma_{11}}{\alpha_1^2} + \frac{\alpha_2^2}{\alpha_1^2}I_2 = I_1 \qquad \text{....(3.74)}$$

Integrating equation (3.74) across the cross-section and the integral of σ_{11} is

zero, when $s = \frac{t-t'}{\alpha_T t_n}$ and $\xi = \frac{r}{R}$ $\qquad \text{....(3.75)}$

$$\int_0^A \frac{\alpha_2^2}{\alpha_1^2} da = 1 + \frac{16v^2}{R^2} \frac{\displaystyle\int_0^{\frac{t}{\alpha_T t_n}} \int_0^1 \exp(-s)*(t - \alpha_T t_n s)^2 (\xi)^2 2\xi d\xi ds}{\displaystyle\int_0^{\frac{t}{\alpha_T t_n}} \int_o^1 \exp(-s) 2\xi d\xi ds} \quad \text{....(3.76)}$$

For a capillary die [12]

$$\int_0^A \frac{\alpha_2^2}{\alpha_1^2} da = B^6 \quad \text{....(3.77)}$$

$$B^6 = 1 + 16\frac{v^2}{R^2}\alpha_T^2 t_n^2 \quad \text{....(3.78)}$$

Introducing equations (3.38), (3.57) and (3.62) in (3.78), the die swell is expressed as

$$B^6 = \left[1 + \left(\frac{N_1}{4\tau_w}\right)^2\right] + \left[\frac{1 + \gamma_1 \alpha_T t_n}{1 - 2\gamma_1 \alpha_T t_n}\right] + \left[1 + 16\frac{v^2}{R^2}\alpha_T^2 t_n^2\right] \quad \text{....(3.79)}$$

where B, N_1, τ_w, γ_1, α_T, t_n, v and R are die swell, first normal stress difference, wall shear stress, average shear rate, shift factor, relaxation time, average velocity of flow and radius of die respectively.

CHAPTER 4
RESULTS AND DISCUSSTION

4.1 Viscous Effect in Melt Flow: Viscosity Versus Shear Rate

Extensive literature survey [8-44] and proposed model (equation number 3.79) indicate the dependency of die swell on viscoelastic properties. To understand this dependency on viscosity of low density polyethylene, polypropylene and polystyrene (amorphous and crystalline) was measured over a wide range of shear rate (0.01 to 400 s^{-1}) and temperature (150 to 290°C) under steady shear condition. Representative plots of steady shear viscosity versus shear rate for amorphous and crystalline polystyrene are shown in Figures 4.1 and 4.2. It is expected that (1) the viscosity of amorphous and crystalline polystyrene remains constant with increasing shear rate in the Newtonian region; then decreases with an increase of shear rate in the non-Newtonian region and finally it attains plateau value. (2) the rate of change of viscosity of polystyrene (both amorphous and crystalline) with shear rate shows three regions i.e. (a) low shear rate region, where it does not change or changes at a very slow rate, (b) intermediate shear rate region, where the rate of reduction of viscosity is very high and (c) high shear rate region, where it remains constant. This change of viscosity with shear rate is decreased by Power law (1925) [76-78], Bueche (1962) [79-80], Cross (1965) [81-82], Ellis (1977) [83], Carreau (1979) [84], Bingham (1922) [85], Hercshel-Bulkley (1926) [86], Casson (1959) [87], Ferry (1942) [88-89], Spencer and Dillon (1949) [88-89] and Berger's (1998) model.
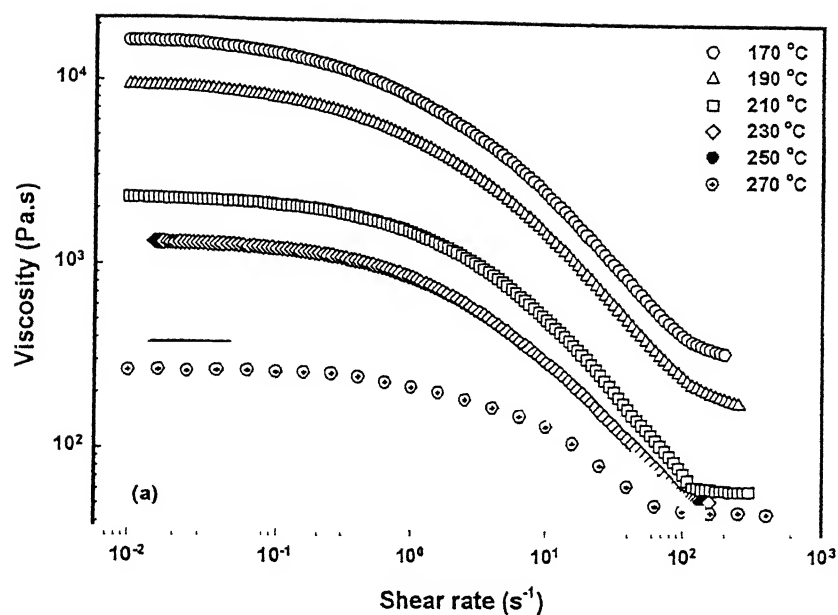
Fig. 4.1 *Steady shear viscosity versus shear rate for amorphous polystyrene.*
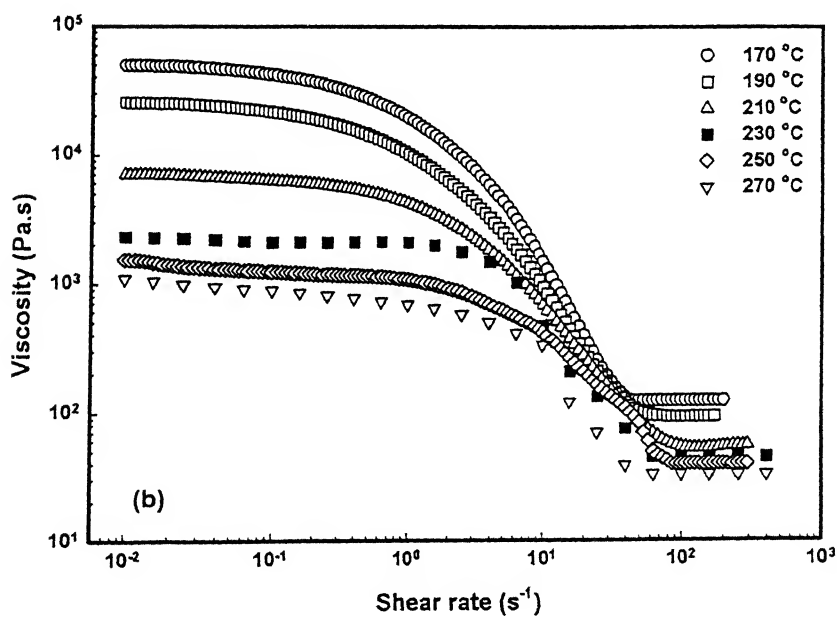
Fig. 4.2 *Steady shear viscosity versus shear rate for crystalline polystyrene.*

Power law Model (1925) [76-78]: This Power law model is developed to describe the dependence of viscosity on shear rate at intermediate shear rate region. It is represented as

$$\tau = k\left(\gamma\right)^{n} \qquad \qquad ....(4.1)$$

or

$$\eta = k\left(\gamma\right)^{n-1} \qquad \qquad ....(4.2)$$

where τ, η and γ are the shear stress, viscosity and shear rate respectively. k and n are two fitting parameters known as consistency index and flow behaviour index. The disadvantages of this model is that the unit of k depends on the value of n. In addition to this, the power law model can not describe the variation of viscosity with shear rate at low and high shear rate region. These fitting parameters (consistency index and flow behaviour index) are evaluated by curve fitting using measured values of viscosity and shear rate over a range of temperature. Tables 4.1-4.8 show the value of consistency index and flow behaviour index (k and n) for low density polyethylene, polypropylene and polystyrene (both amorphous and crystalline). The consistency index decreases with an increase of temperature for both the materials. But there is no particular trend for the flow behaviour index. A representative curve for low density polyethylene at 270°C is shown in Figure 4.3.

Table 4.1: Consistency index (k) and flow behaviour index (n) for low density polyethylene. Equation 4.1 is used to find out these parameters. R is a regression coefficient.

Temperature (°C)	k	n	R^2
210	8198.58	0.29	0.9445
230	5606.46	0.31	0.9646
250	3224.08	0.38	0.9905
270	1991.53	0.41	0.9932
290	749.63	0.30	0.9599

Table 4.2: Consistency index (k) and flow behaviour index (n) for low density polyethylene. Equation 4.2 is used to find out these parameters. R is a regression coefficient.

Temperature (°C)	k	n	R^2
210	6089.25	0.40	0.9522
230	4086.44	0.43	0.9483
250	3397.75	0.46	0.9738
270	1579.81	0.49	0.9781
290	625.76	0.36	0.9827

Table 4.3: Consistency index (k) and flow behaviour index (n) for polypropylene. Equation 4.1 is used to find out these parameters. R is a regression coefficient.

Temperature (°C)	k	n	R^2
170	2991.44	0.30	0.8223
190	2466.37	0.29	0.7403
210	997.72	0.57	0.9931
230	748.92	0.35	0.7290
250	537.64	0.37	0.8553
270	277.31	0.26	0.6590
290	10.29	0.92	0.9990

Table 4.4: Consistency index (k) and flow behaviour index (n) for polypropylene. Equation 4.2 is used to find out these parameters. R is a regression coefficient.

Temperature (°C)	k	n	R^2
170	1672.34	0.49	0.8432
190	1158.23	0.53	0.7907
210	459.44	0.66	0.6349
230	277.34	0.64	0.6343
250	195.45	0.68	0.6509
270	133.41	0.42	0.8452
290	3.44	0.37	0.0775

Table 4.5: Consistency index (k) and flow behaviour index (n) for amorphous polystyrene. Equation 4.1 is used to find out these parameters. R is a regression coefficient.

Temperature (°C)	k	n	R^2
170	3812.78	0.81	0.9929
190	178.95	0.98	0.7651
210	751.93	0.30	0.4934
230	282.68	0.47	0.7759
250	55.64	0.92	0.9119
270	52.16	0.90	0.9821
290	49.53	0.71	0.9728

Table 4.6: Consistency index (k) and flow behaviour index (n) for amorphous polystyrene. Equation 4.2 is used to find out these parameters. R is a regression coefficient.

Temperature (°C)	k	n	R^2
170	3899.51	0.86	0.8133
190	965.67	0.62	0.7547
210	195.24	0.78	0.3984
230	71.75	0.84	0.2871
250	56.83	0.93	0.4524
270	53.22	0.90	0.8496
290	25.85	0.89	0.8607

Table 4.7: Consistency index (k) and flow behaviour index (n) for crystalline polystyrene. Equation 4.1 is used to find out these parameters. R is a regression coefficient.

Temperature (°C)	k	n	R^2
190	6895.42	0.23	0.7105
210	3316.56	0.29	0.6892
230	1560.40	0.43	0.7668
250	1088.91	0.29	0.5827
270	514.81	0.52	0.9283
290	329.98	0.55	0.9634

Table 4.8: Consistency index (k) and flow behaviour index (n) for crystalline polystyrene. Equation 4.2 is used to find out these parameters. R is a regression coefficient.

Temperature (°C)	k	n	R^2
190	4209.17	0.40	0.8780
210	538.25	0.61	0.5249
230	349.14	0.87	0.4389
250	360.15	0.57	0.6107
270	215.50	0.76	0.7805
290	160.51	0.79	0.8990
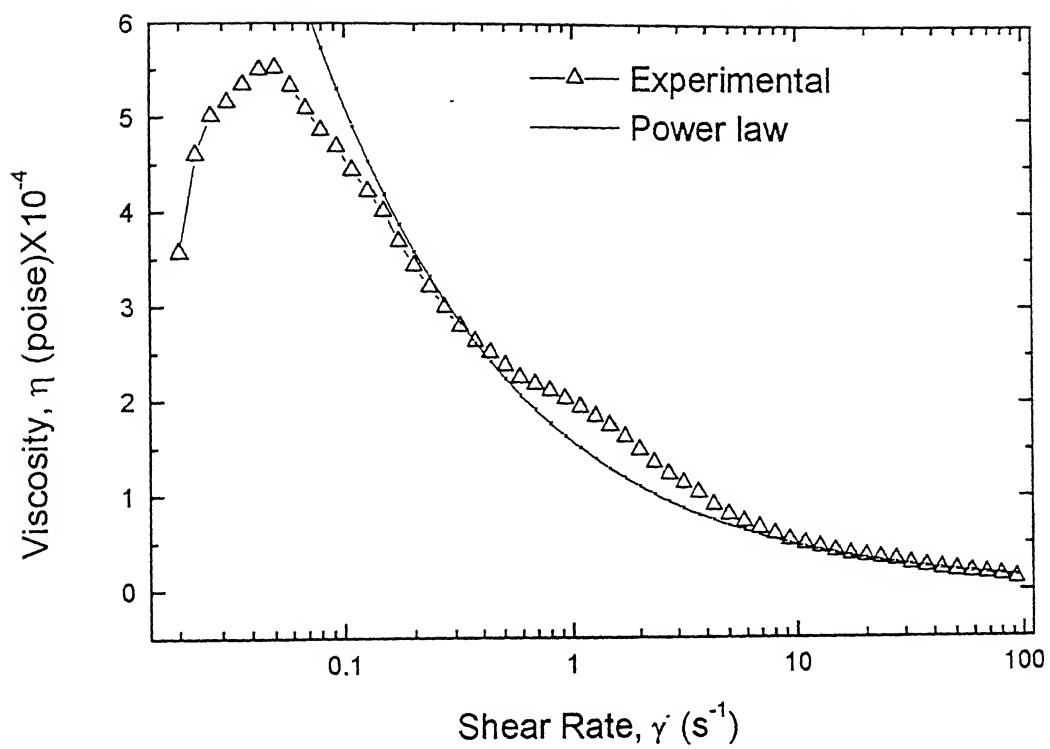
Fig. 4.3 *A representative best fit curve for Power law model (low density polyethylene at 270°C).*

Table 4.10: Bueche's parameter η_0, a, λ and b for polypropylene. These parameters are obtained from equation 4.3. R is a regression coefficient.

Temperature (°C)	η_0	a	λ	b	R^2
170	3765.19	1.09	0.32	0.99	0.9956
190	2240.99	0.77	0.31	0.91	0.9909
210	758.45	0.75	0.11	1.17	0.9938
230	418.30	1.15	0.06	1.84	0.9923
250	288.05	0.17	0.002	2.70	0.9894
270	925.92	2.60	4.34	0.39	0.9690
290	9.55	0.32	6.34	-13.10	0.6918

Table 4.11: Bueche's parameter η_0, a, λ and b for amorphous polystyrene. These parameters are obtained from equation 4.3. R is a regression coefficient.

Temperature (°C)	η_0	a	λ	b	R^2
170	4694.92	2.12	0.27	1.91	0.9268
190	1475.77	0.71	0.15	1.23	0.9913
210	243.85	0.76	0.03	2.86	0.9885
230	78.78	0.84	0.02	4.26	0.9308
250	60.10	0.42	0.02	1.79	0.7857
270	64.42	0.65	0.04	0.55	0.9506
290	38.06	0.79	0.10	0.28	0.9356

Table 4.12: Bueche's parameter η_0, a, λ and b for crystalline polystyrene. These parameters are obtained from equation 4.3. R is a regression coefficient.

Temperature (°C)	η_0	a	λ	b	R^2
190	12523.01	1.09	0.67	0.87	0.9945
210	1868.61	0.001	0.28	3.90	0.9839
230	1792.67	2.39	5.61	0.70	0.9751
250	510.11	0.49	0.11	1.34	0.9621
270	385.74	0.92	0.27	0.45	0.9687
290	293.54	0.91	0.36	0.46	0.9846
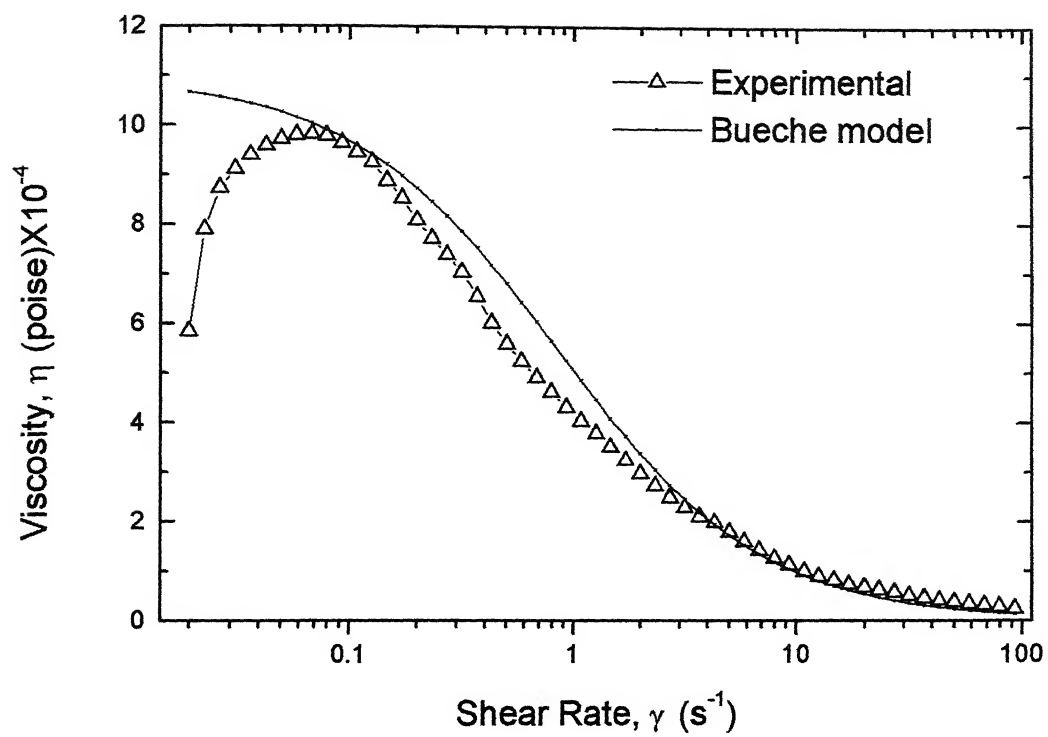
Fig. 4.4 *A representative best fit curve for Bueche model (low density polyethylene at 250°C).*

Cross Model (1965) [81-82]: In order to eliminate the disadvantages of Power law model and to establish a correlation between these fitting parameters, number of generalized equations have been developed. Cross is one of these models. This is a three parameter model given by

$$\eta = \frac{\eta_0}{\left(1 + k\gamma\right)^{1-n}} \qquad ....(4.4)$$

where η and γ are viscosity and shear rate respectively. The other parameters η_0, k and n are fitting parameter and given in Tables 4.13–4.16 for low density polyethylene, polypropylene and polystyrene (both amorphous and crystalline) respectively. The zero shear viscosity decreases with an increase of temperature for both materials. But the other parameters vary independently with temperature. Figure 4.5 shows a representative best fit curve for crystalline polystyrene at 190°C.

Table 4.13: Cross parameters η_0, k and n for low density polyethylene. These are obtained from equation 4.4. R is a regression coefficient.

Temperature (°C)	η_0	k	n	R^2
210	18353.40	1.11	0.03	0.9965
230	11181.70	0.88	0.001	0.9944
250	10974.10	1.62	0.16	0.9952
270	7259.65	5.14	0.36	0.9922
290	11031.30	52.32	0.25	0.9577

Table 4.14: Cross parameters η_0, k and n for polypropylene. These are obtained from equation 4.4. R is a regression coefficient.

Temperature (°C)	η_0	k	n	R^2
170	3765.19	0.35	0.01	0.9956
190	2240.99	0.23	0.09	0.9909
210	753.67	11.60	2.19	0.9942
230	418.81	0.07	-0.84	0.9909
250	288.05	6.08	-1.70	0.9898
270	849.84	34.27	0.60	0.9684
290	7.94	14.18	8.42	0.5280

Table 4.15: Cross parameters η_0, k and n for amorphous polystyrene. These are obtained from equation 4.4. R is a regression coefficient.

Temperature (°C)	η_0	k	n	R^2
170	4694.93	0.41	-0.91	0.9268
190	1478.36	0.12	-0.22	0.9912
210	243.28	0.03	-1.88	0.9868
230	78.59	0.01	-3.28	0.9234
250	59.94	0.01	-0.82	0.8544
270	63.66	0.02	0.42	0.9538
290	32.51	0.02	0.60	0.8761

Table 4.16: Cross parameters η_0, k and n for crystalline polystyrene. These are obtained from equation 4.4. R is a regression coefficient.

Temperature (°C)	η_0	k	n	R^2
190	12523.20	0.74	0.13	0.9945
210	1942.07	0.10	-2.82	0.9839
230	827.02	0.06	-0.65	0.9751
250	510.09	0.06	-0.34	0.9621
270	385.38	0.23	0.54	0.9687
290	293.54	0.29	0.54	0.9896
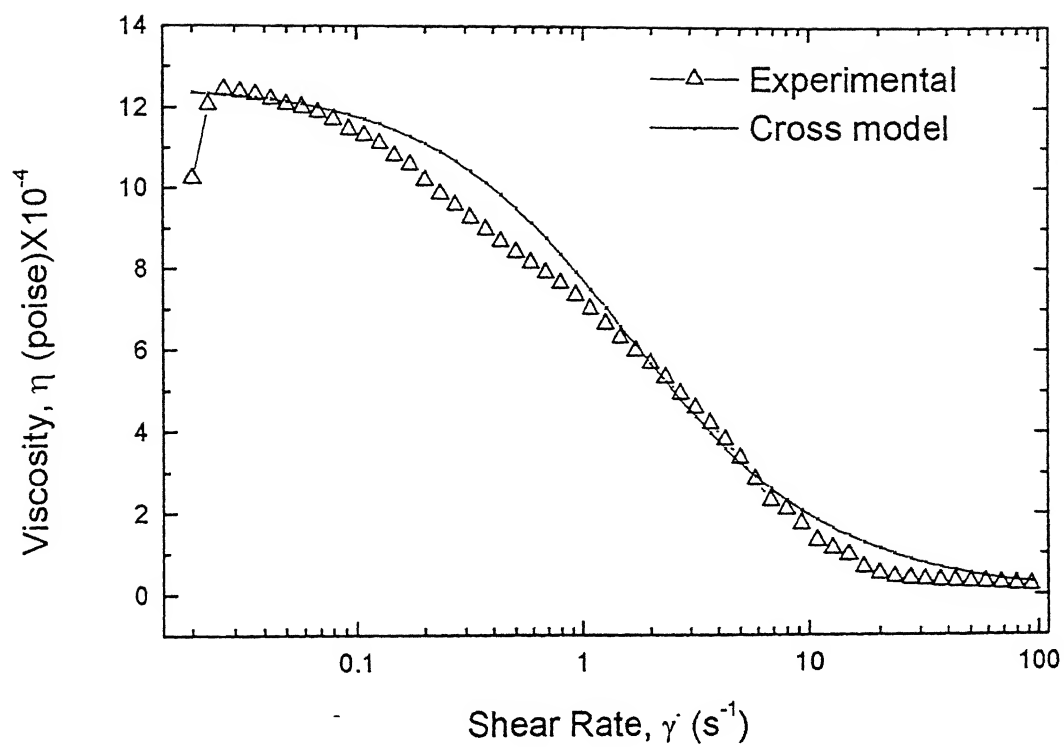
Fig. 4.5 *A representative best fit curve for Cross model (crystalline polystyrene at 190°C).*

Ellis Model (1977) [83]: Ellis has proposed a three parameter model to eliminate the drawback of Power law model. This is represented as

$$\eta_{app} = \frac{\eta_0}{1 + \left(\dfrac{\tau}{\tau_{1/2}}\right)^{a-1}} \qquad \text{....}(4.5)$$

where η_{app} and τ are the apparent viscosity and shear stress respectively. And the other parameters η_0, $\tau_{1/2}$ and a are viscosity at zero shear rate, shear stress where viscosity is $\eta_0/2$ and a dimensionless fitting parameter respectively. Similarly these fitting parameters zero shear viscosity, shear stress where viscosity is $\eta_0/2$ and dimensionless fitting parameter are obtained from curve fitting and given in Tables 4.17-4.20 for low density polyethylene, polypropylene and polystyrene (both amorphous and crystalline) respectively. The same trend i.e. the decrease of zero shear viscosity as observed in Cross model is also observed here. A representative best fit curve for amorphous polystyrene at 190°C is shown in Figure 4.6.

Table 4.17: Ellis parameters: zero shear viscosity, shear stress where viscosity is $\eta_0/2$ and fitting parameter for low density polyethylene. These parameters are obtained from equation 4.5. R is a regression coefficient.

Temperature (°C)	η_0	$\tau_{1/2}$	a	R^2
210	17747.41	0.99	2.02	0.9939
230	11181.70	1.13	1.99	0.9944
250	10602.90	0.68	1.87	0.9934
270	7259.65	0.19	1.64	0.9922
290	11544.71	0.01	1.67	0.9568

Table 4.18: Ellis parameters: zero shear viscosity, shear stress where viscosity is $\eta_0/2$ and fitting parameter for polypropylene. These parameters are obtained from equation 4.5. R is a regression coefficient.

Temperature (°C)	η_0	$\tau_{1/2}$	a	R^2
170	3776.19	2.85	1.99	0.9955
190	2245.03	4.22	1.90	0.9907
210	753.67	11.59	2.18	0.9942
230	418.90	14.22	2.83	0.9918
250	288.05	1643.43	3.70	0.9460
270	849.84	0.03	1.40	0.9684
290	7.94	0.07	-6.42	0.5280

Table 4.19: Ellis parameters: zero shear viscosity, shear stress where viscosity is $\eta_0/2$ and fitting parameter for amorphous polystyrene. These parameters are obtained from equation 4.5. R is a regression coefficient.

Temperature (°C)	η_0	$\tau_{1/2}$	a	R^2
170	4694.93	2.46	2.91	0.9268
190	1475.79	8.50	2.23	0.9913
210	243.31	31.07	3.88	0.9881
230	76.78	54.67	5.26	0.9308
250	60.10	74.65	2.79	0.7857
270	65.34	49.01	1.53	0.9470
290	38.06	23.52	1.28	0.9356

Table 4.20: Ellis parameters: zero shear viscosity, shear stress where viscosity is $\eta_0/2$ and fitting parameter for crystalline polystyrene. These parameters are obtained from equation 4.5. R is a regression coefficient.

Temperature (°C)	η_0	$\tau_{1/2}$	a	R^2
190	12523.20	1.35	1.87	0.9945
210	1942.07	10.07	4.82	0.9839
230	714.21	25.50	6.65	0.9751
250	508.09	15.69	2.36	0.9617
270	376.86	4.94	1.47	0.9685
290	293.54	3.43	1.46	0.9891
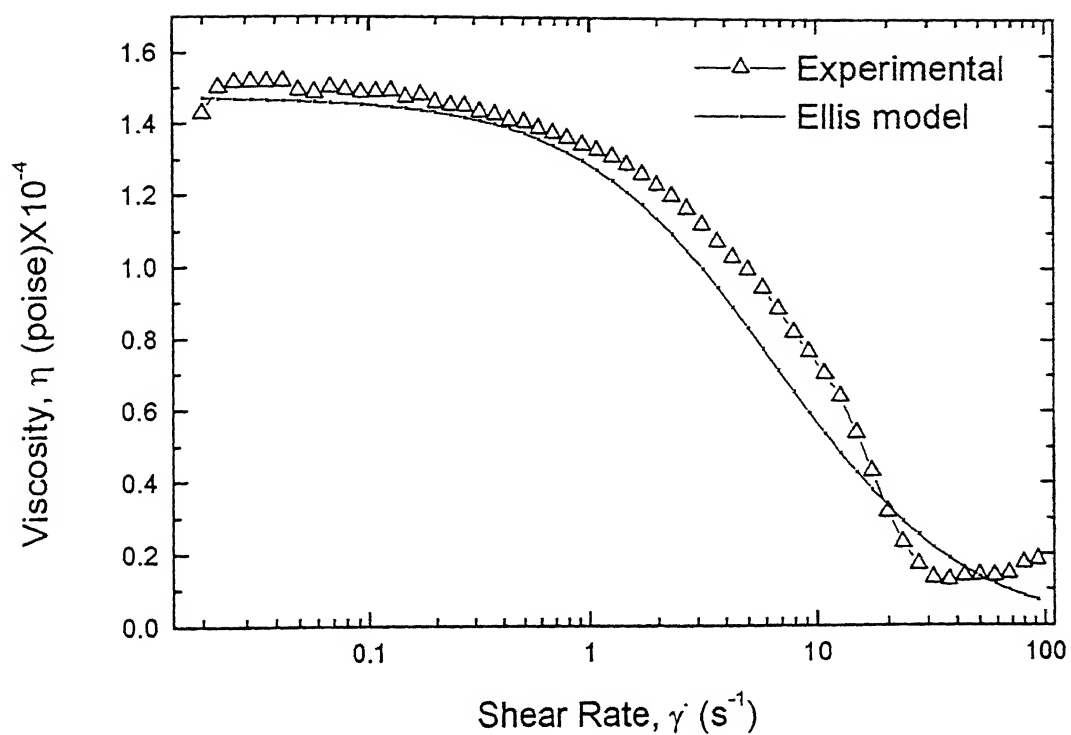
Fig. 4.6 *A representative best fit curve for Ellis model (amorphous polystyrene at 190°C).*

Carreau's Model (1979) [84]: A four parameter viscosity model to predict the viscosity over a wide range of shear rate (low-intermediate-high) has been proposed by Carreau. This four parameter viscosity model is represented by

$$\eta = \frac{\eta_0}{\left[1+\left(\lambda\gamma\right)^a\right]^{\frac{1-b}{a}}} \qquad \text{....(4.6)}$$

where η and γ are viscosity and shear rate respectively. The other parameters η_0, λ, a and b are fitting parameters and obtained from curve fitting. These parameters are given in Tables 4.21-4.24 for low density polyethylene, polypropylene and polystyrene (both amorphous and crystalline) respectively. A representative best fit curve of Carreau model for polypropylene at 170°C is shown in Figure 4.7. Here, zero shear viscosity, η_0 (Carreau parameter) decreases with an increase of temperature. Same trend is also observed in Cross model and Ellis model. But the other parameters change independently with temperature.

Table 4.21: Carreau parameter η_0, λ, a and b for low density polyethylene. These are obtained from equation 4.6. R is a regression coefficient.

Temperature (°C)	η_0	λ	a	b	R^2
210	17734.31	2.80	1.56	0.34	0.9988
230	10959.80	2.51	1.66	0.35	0.9986
250	9886.52	5.11	2.13	0.46	0.9987
270	7009.93	10.41	0.83	0.46	0.9946
290	176470	188.22	0.22	0.11	0.9622

Table 4.22: Carreau parameter η_0, λ, a and b for polypropylene. These are obtained from equation 4.6. R is a regression coefficient.

| Temperature (°C)	η_0	λ	a	b	R^2
170	3891.38	0.03	0.72	-1.78	0.9980
190	2327.56	0.01	0.62	-3.62	0.9958
210	761.60	0.06	1.06	-0.43	0.9942
230	418.36	0.11	2.13	-0.13	0.9884
250	363.61	1.00	0.50	0.20	0.9902
270	1511.38	1.37	0.20	0.38	0.9703
290	7.85	0.01	5.47	-5.02	0.0001

Table 4.23: Carreau parameter η_0, λ, a and b for amorphous polystyrene. These are obtained from equation 4.6. R is a regression coefficient.

Temperature (°C)	η_0	λ	a	b	R^2
170	4689.38	0.54	2.02	-0.30	0.9274
190	1492.54	0.03	0.98	-1.54	0.9929
210	244.42	0.01	2.06	-12.04	0.9899
230	78.43	0.02	6.03	-2.33	0.9259
250	60.33	0.01	1.49	-5.93	0.7953
270	66.31	0.002	0.45	-0.16	0.9515
290	33.52	0.16	0.43	0.76	0.9138

Table 4.24: Carreau parameter η_0, λ, a and b for crystalline polystyrene. These are obtained from equation 4.6. R is a regression coefficient.

Temperature (°C)	η_0	λ	a	b	R^2
190	13428.40	0.03	0.57	-2.05	0.9978
210	1815.88	0.61	11.39	-0.44	0.9901
230	830.18	0.23	9.91	-1.31	0.9838
250	522.00	0.000361	0.89	-60.22	0.9739
270	392.82	0.01	0.36	-0.02	0.9713
290	299.26	0.13	0.42	0.45	0.9868
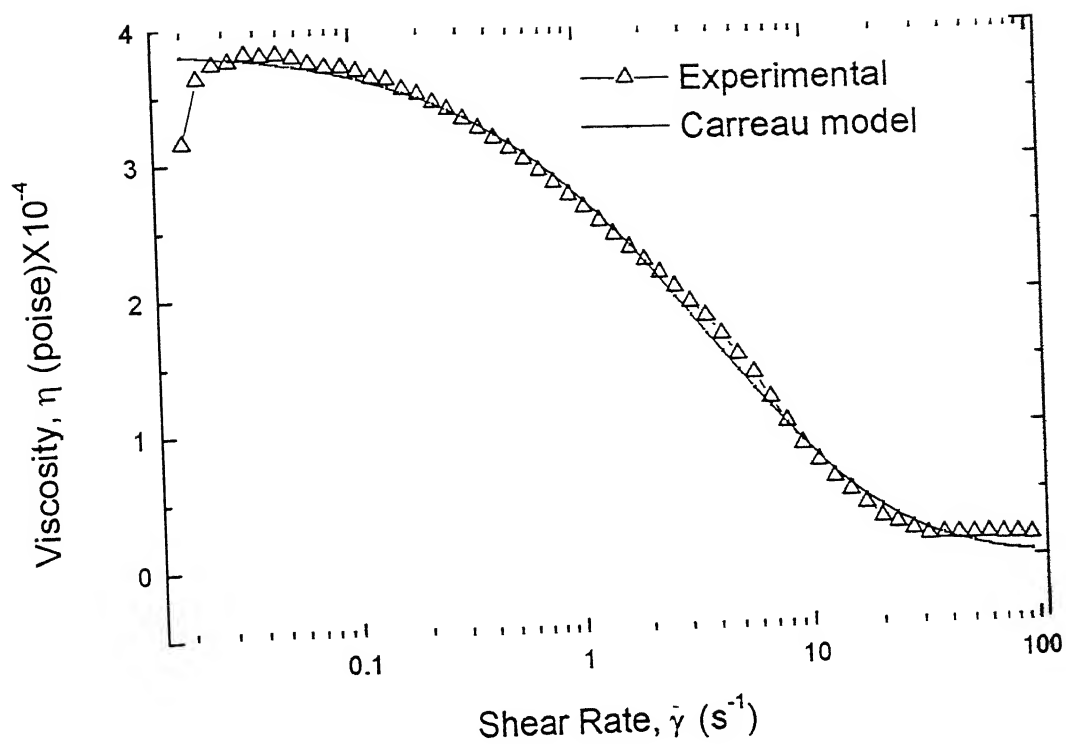
Fig. 4.7 *A representative best fit curve for Carreau model (polypropylene at 170°C).*

Bingham's Model (1922) [85]: A different type of model has been proposed by Bingham to explain the change of viscosity with shear rate for a material that shows yield behavior during flow. In this case the material withstands a certain amount of stress without deformation. The maximum shear stress that can be sustained without flow is known as yield stress. This is given by

$$\tau = \tau_y + \eta_p \gamma \qquad \qquad ....(4.7)$$

$$\eta = \eta_p + \frac{\tau_y}{\gamma} \qquad \qquad ....(4.8)$$

where τ, η and γ are shear stress, viscosity and shear rate respectively. The other parameters τ_y and η_p (yield stress and plastic viscosity) known as fitting parameters and obtained by curve fitting. These are given in Tables 4.25-4.32 for low density polyethylene, polypropylene and polystyrene (both amorphous and crystalline). The equations 4.7 and 4.8 are not constitutive equations, as they do not describe all the components of the stress tensor in any type of deformations. It is only used in simple shear flow. A representative best fit curve for low density polyethylene at 290°C is shown in Figure 4.8. The yield stress and plastic viscosity generally decreases with increasing temperature for both the materials (low density polyethylene, polypropylene and polystyrene).

Table 4.25: Bingham's parameter τ_y and η_p for low density polyethylene. These fitting parameters are obtained from equation 4.7. R is a regression coefficient.

Temperature (°C)	τ_y	η_p	R^2
210	7420.68	308.01	0.5819
230	5006.36	250.86	0.6622
250	3863.90	271.30	0.7842
270	1855.46	144.08	0.7926
290	697.63	30.12	0.6446

Table 4.26: Bingham's parameter τ_y and η_p for low density polyethylene. These fitting parameters are obtained from equation 4.8. R is a regression coefficient.

Temperature (°C)	τ_y	η_p	R^2
210	1074.72	4337.36	0.6831
230	652.59	2974.56	0.6459
250	493.89	2119.85	0.7633
270	273.60	1041.67	0.8161
290	161.09	349.63	0.9547

Table 4.27: Bingham's parameter τ_y and η_p for polypropylene. These fitting parameters are obtained from equation 4.7. R is a regression coefficient.

Temperature (°C)	τ_y	η_p	R^2
170	2624.76	126.86	0.5595
190	2203.98	90.66	0.3894
210	574.17	230.83	0.9052
230	633.89	42.81	0.5196
250	415.01	40.89	0.5822
270	260.62	7.26	0.2258
290	3.57	7.52	0.9973

Table 4.28: Bingham's parameter τ_y and η_p for polypropylene. These fitting parameters are obtained from equation 4.8. R is a regression coefficient.

Temperature (°C)	τ_y	η_p	R^2
170	84.23	1698.96	0.3864
190	120.15	838.81	0.4035
210	47.64	355.93	0.3951
230	13.56	124.92	0.3771
250	8.22	118.92	0.3819
270	16.34	105.29	0.7539
290	-0.66	9.81	0.5452

Table 4.29: Bingham's parameter τ_y and η_p for amorphous polystyrene. These fitting parameters are obtained from equation 4.7. R is a regression coefficient.

Temperature (°C)	τ_v	η_p	R^2
170	341.54	3417.67	0.9808
190	1618.77	145.62	0.7043
210	198.42	140.72	0.8759
230	54.14	61.88	0.9473
250	0.94	47.44	0.8918
270	0.83	43.10	0.9683
290	34.11	14.49	0.9321

Table 4.30: Bingham's parameter τ_y and η_p for amorphous polystyrene. These fitting parameters are obtained from equation 4.8. R is a regression coefficient.

Temperature (°C)	τ_v	η_p	R^2
170	68.58	4082.36	0.2909
190	33.25	1054.84	0.3040
210	1.07	228.88	0.1370
230	0.06	76.71	0.0307
250	1.07	47.22	0.1256
270	1.26	42.37	0.4235
290	0.69	22.74	0.4861

Table 4.31: Bingham's parameter τ_y and η_p for crystalline polystyrene. These fitting parameters are obtained from equation 4.7. R is a regression coefficient.

Temperature (°C)	τ_v	η_p	R^2
190	6202.56	180.56	0.3660
210	2524.40	174.02	0.7118
230	808.89	253.49	0.7253
250	996.31	34.92	0.2156
270	390.59	69.30	0.7785
290	270.89	48.80	0.8527

Table 4.32: Bingham's parameter τ_y and η_p for crystalline polystyrene. These fitting parameters are obtained from equation 4.8. R is a regression coefficient.

Temperature (°C)	τ_y	η_p	R^2
190	428.62	4056.72	0.5367
210	13331.20	39.75	0.3902
230	34.10	0.11	0.2257
250	14.03	3330.45	0.2929
270	7.11	193.19	0.4453
290	3.93	145.83	0.4685
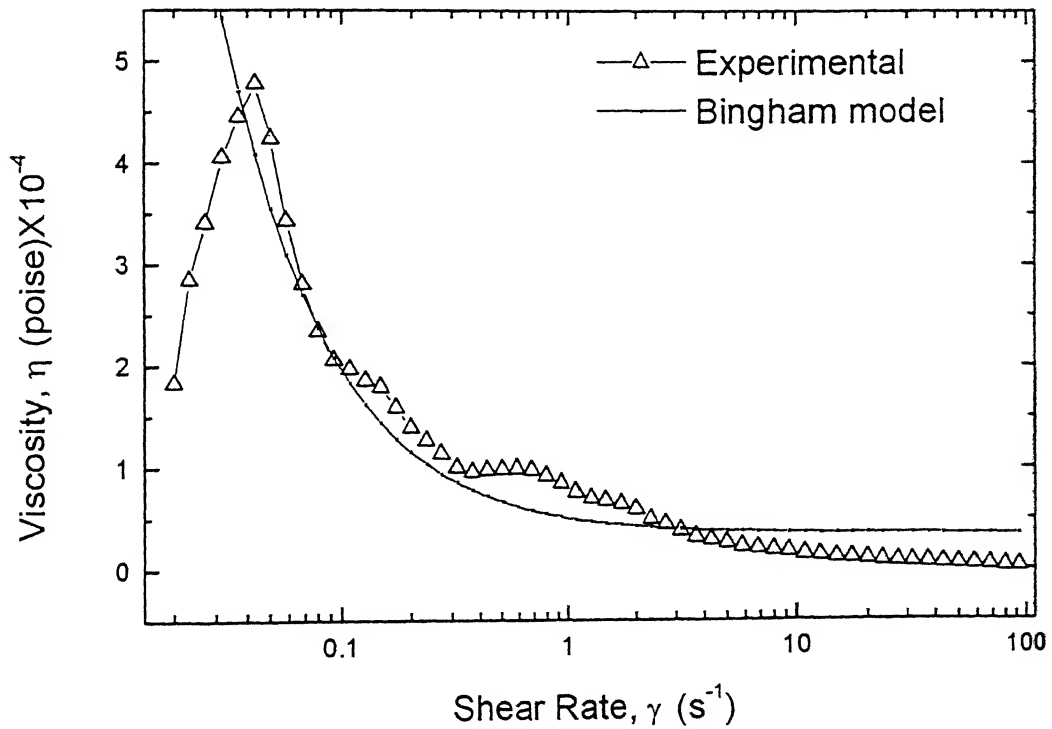
Fig. 4.8 *A representative best fit curve for Bingham model (low density polyethylene at 290°C).*

Herschel-Bulkley Model (1926) [86]: To fit the experimental data of viscosity versus shear rate in a better way, Herschel and Bulkley have proposed a three parameter model. This is represented by

$$\tau = \tau_y + k\left(\gamma\right)^{n-1} \qquad \text{....(4.9)}$$

or

$$\eta = \frac{\tau_y}{\gamma} + k\gamma^{n-2} \qquad \text{....(4.10)}$$

where τ, η and γ are shear stress, viscosity and shear rate respectively. The other parameters τ_y, k and n (yield stress, plastic viscosity and power law index respectively) are obtained from curve fitting and given in Tables 4.33-4.40 for low density polyethylene, polypropylene and polystyrene (both amorphous and crystalline). The third parameter n (power law index) helps to fit the experimental data in a better way. A representative best fit plot of viscosity versus shear rate for crystalline polystyrene at 190°C is shown in Figure 4.9.

Table 4.33: Herschel-Bulkley's parameter τ_y, k and n for low density polyethylene. Equation 4.9 is used to calculate these parameter. R is a regression coefficient.

Temperature (°C)	τ_y	k	n	R^2
210	1.00	1.00	2.00	0.5854
230	1.00	1.00	2.00	0.6637
250	1.00	1.00	2.00	0.8069
270	1.00	1.00	2.00	0.7962
290	1.00	1.00	2.00	0.6446

Table 4.34: Herschel-Bulkley's parameter τ_y, k and n for low density polyethylene. Equation 4.10 is used to calculate these parameter. R is a regression coefficient.

Temperature (°C)	τ_y	k	n	R^2
210	-1110.80	8916.52	1.50	0.9896
230	-633.22	5846.69	1.53	0.9847
250	-606.90	4681.90	1.48	0.9954
270	-289.49	2082.45	1.45	0.9946
290	-266.98	910.84	1.25	0.9399

Table 4.35: Herschel-Bulkley's parameter τ_y, k and n for polypropylene. Equation 4.9 is used to calculate these parameter. R is a regression coefficient.

Temperature (°C)	τ_y	k	n	R^2
170	1.00	1.00	2.00	0.5595
190	1.00	1.00	2.00	0.3861
210	1.00	1.00	0.00	0.9084
230	685.68	36.34	1.99	0.3873
250	-696.68	1066.46	1.18	0.8309
270	216.91	74.22	1.39	0.5042
290	0.53	9.30	1.58	0.9565

Table 4.36: Herschel-Bulkley's parameter τ_y, k and n for polypropylene. Equation 4.10 is used to calculate these parameter. R is a regression coefficient.

Temperature (°C)	τ_y	k	n	R^2
170	-121.18	2390.84	1.67	0.9375
190	-85.67	1583.26	1.69	0.9297
210	-27.24	666.85	1.79	0.8531
230	-14.83	379.75	1.78	0.7653
250	-5.62	248.02	1.81	0.8514
270	-3.19	164.82	1.66	0.9673
290	-0.59	10.26	1.94	0.7340

Table 4.37: Herschel-Bulkley's parameter τ_y, k and n for amorphous polystyrene. Equation 4.9 is used to calculate these parameter. R is a regression coefficient.

Temperature (°C)	τ_y	k	n	R^2
170	1.00	1.00	2.00	0.9808
190	1.00	1.00	2.00	0.7043
210	1.00	1.00	2.00	0.2701
230	1.00	1.00	2.00	0.7405
250	2.53	24.01	2.11	0.8614
270	1.95	25.04	2.08	0.9554
290	61.91	5.62	2.21	0.8839

Table 4.38: Herschel-Bulkley's parameter τ_y, k and n for amorphous polystyrene. Equation 4.10 is used to calculate these parameter. R is a regression coefficient.

Temperature (°C)	τ_y	k	n	R^2
170	2364.73	-38.96	-1.24	0.8692
190	-46.69	1195.54	1.75	0.8575
210	-3.41	234.89	1.89	0.5675
230	-0.78	78.22	1.93	0.3334
250	-0.58	58.18	1.91	0.4867
270	-0.55	55.43	1.88	0.8439
290	-0.37	27.34	1.89	0.9208

Table 4.39: Herschel-Bulkley's parameter τ_y, k and n for crystalline polystyrene. Equation 4.9 is used to calculate these parameter. R is a regression coefficient.

Temperature (°C)	τ_y	k	n	R^2
190	1.00	1.00	2.00	0.3634
210	*	*	*	*
230	*	*	*	*
250	746.47	89.84	2.42	0.7630
270	1.00	1.00	2.00	0.6491
290	*	*	*	*

Table 4.40: Herschel-Bulkley's parameter τ_y, k and n for crystalline polystyrene. Equation 4.10 is used to calculate these parameter. R is a regression coefficient.

Temperature (°C)	τ_y	k	n	R^2
190	-414.18	6433.85	1.61	0.9648
210	-49.34	1719.72	1.75	0.8585
230	-14.07	700.39	1.81	0.7453
250	-8.86	429.48	1.81	0.7891
270	-4.49	245.02	1.81	0.9541
290	-3.23	179.27	1.79	0.9709
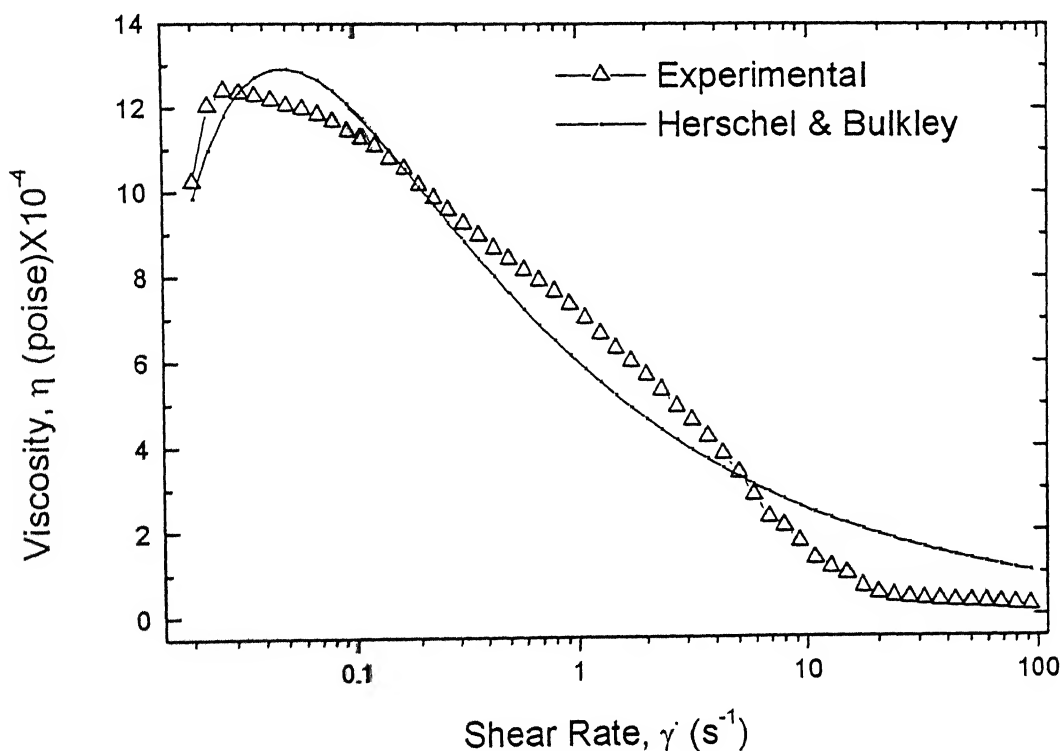
Fig. 4.9 *A representative best fit curve for Herschel-Bulkley model (crystalline polystyrene at 190°C).*

68

Casson's Model (1959) [87]: This model is an extension of Bingham model. It is also two parameter model gives a better fit to the experimental data compared with Bingham model. This is represented by

$$\sqrt{\tau} = \sqrt{\tau_y} + \sqrt{\eta_p \gamma} \qquad \text{....(4.11)}$$

or

$$\sqrt{\eta} = \sqrt{\eta_p} + \frac{\sqrt{\tau_y}}{\sqrt{\gamma}} \qquad \text{....(4.12)}$$

where τ, η and γ are shear stress, viscosity and shear rate respectively. The other parameters τ_y, η_p (yield stress and plastic viscosity) are obtained from curve fitting and given in Tables 4.41-4.48 for low density polyethylene, polypropylene and both polystyrenes. Figure 4.10 describes the best fit data on the Casson model for low density polyethylene at 290°C as a representative. The same trend as observed in Bingham models, the decrease of yield stress and plastic viscosity is also observed here.

Table 4.41: Casson's parameter τ_y and η_p for low density polyethylene. These parameters are obtained from equation 4.11. R is a regression coefficient.

Temperature (°C)	$\sqrt{\tau_y}$	$\sqrt{\eta_p}$	R^2
210	24.36	24.82	0.7079
230	18.41	22.39	0.7523
250	17.26	22.24	0.8460
270	13.06	15.70	0.8678
290	11.46	6.69	0.7775

Table 4.42: Casson's parameters τ_y and η_p for low density polyethylene. These parameters are obtained from equation 4.12. R is a regression coefficient.

Temperature (°C)	$\sqrt{\tau_y}$	$\sqrt{\eta_p}$	R^2
210	3936.10	2332.43	0.8416
230	2384.93	1743.80	0.8058
250	2169.06	1182.63	0.8748
270	1069.02	497.63	0.9365
290	809.40	-117.88	0.9561

Table 4.43: Casson's parameter τ_y and η_p for polypropylene. These parameters are obtained from equation 4.11. R is a regression coefficient.

Temperature (°C)	$\sqrt{\tau_y}$	$\sqrt{\eta_p}$	R^2
170	11.34	15.66	0.6537
190	8.39	13.89	0.6079
210	3.56	9.17	0.8522
230	2.96	8.98	0.6816
250	2.78	7.99	0.9341
270	2.45	6.31	0.7190
290	1.28	4.44	0.9292

Table 4.44: Casson's parameter τ_y and η_p for polypropylene. These parameters are obtained from equation 4.12. R is a regression coefficient.

Temperature (°C)	$\sqrt{\tau_y}$	$\sqrt{\eta_p}$	R^2
170	632.14	1156.57	0.6497
190	380.06	795.17	0.6327
210	118.51	386.24	0.4658
230	85.55	214.03	0.4317
250	38.92	164.22	0.3824
270	73.91	63.24	0.9193
290	-2.32	10.60	0.3294

Table 4.45: Casson's parameter τ_y and η_p for amorphous polystyrene. These parameters are obtained from equation 4.11. R is a regression coefficient.

Temperature (°C)	$\sqrt{\tau_y}$	$\sqrt{\eta_p}$	R^2
170	2.90	60.45	0.9873
190	5.74	16.00	0.7645
210	3.15	3.39	0.4656
230	0.42	6.97	0.8258
250	0.33	6.88	0.9624
270	0.40	6.45	0.9831
290	0.22	4.53	0.9782

Table 4.46: Casson's parameter τ_y and η_p for amorphous polystyrene. These parameters are obtained from equation 4.12. R is a regression coefficient.

Temperature (°C)	$\sqrt{\tau_y}$	$\sqrt{\eta_p}$	R^2
170	552.39	3448.51	0.6371
190	288.17	639.86	0.5340
210	25.54	173.41	0.2396
230	4.21	67.27	0.1136
250	6.01	43.95	0.4377
270	7.77	38.38	0.6533
290	2.11	21.81	0.5436

Table 4.47: Casson's parameter τ_y and η_p for crystalline polystyrene. These parameters are obtained from equation 4.11. R is a regression coefficient.

Temperature (°C)	$\sqrt{\tau_y}$	$\sqrt{\eta_p}$	R^2
190	22.96	18.80	0.5193
210	8.67	17.57	0.5906
230	2.12	21.01	0.8834
250	3.36	11.89	0.7104
270	2.43	9.92	0.8500
290	1.80	9.22	0.9365

Table 4.48: Casson's parameter τ_y and η_p for crystalline polystyrene. These parameters are obtained from equation 4.12. R is a regression coefficient.

Temperature (°C)	$\sqrt{\tau_y}$	$\sqrt{\eta_p}$	R^2
190	2225.04	2547.41	0.7641
210	18.54	33.81	0.4885
230	257.53	-26.47	0.4149
250	57.32	296.38	0.4597
270	39.12	164.81	0.6710
290	39.83	109.17	0.7512
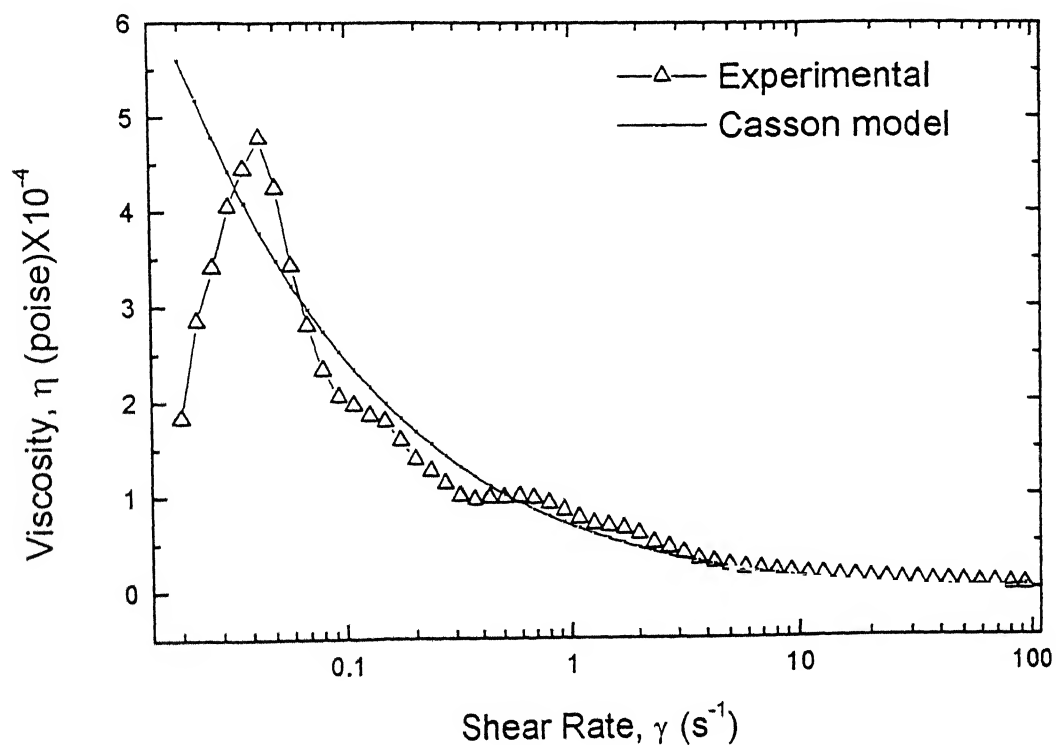
Fig. 4.10 *A representative best fit curve for Casson model (low density polyethylene at 290°C).*

72

Ferry's Model (1942) [88-89]: Ferry's has proposed a model to explain the dependency of viscosity on shear rate with the help of material property (G_i) as

$$\gamma = \frac{\tau}{\eta_0}\left(1 + \frac{\tau}{G_i}\right) \qquad ....(4.13)$$

or

$$\gamma = \frac{\left(\frac{\eta_0}{\eta} - 1\right)G_i}{\eta} \qquad ....(4.14)$$

where τ, γ and η are shear stress, shear rate and viscosity respectively. The other parameters η_0 and G_i are obtained from curve fitting and given in Tables 4.49-4.56 for low density polyethylene, polypropylene and polystyrene (both amorphous and crystalline). Figure 4.11 describes a representative best fit curve for Ferry's model at 190°C for crystalline polystyrene.

Table 4.49: Ferry's parameter η_0 and G_i for low density polyethylene. These parameters are obtained from equation 4.13. R is a regression coefficient.

Temperature (°C)	η_0	G_i	R^2
210	2.73×10^5	49.09	0.7660
230	4.14×10^5	17.57	0.8713
250	1.63×10^5	44.50	0.9733
270	-475.64	-2748.90	0.9513
290	-69.09	-965.06	0.8317

Table 4.50: Ferry's parameter η_0 and G_i for low density polyethylene. These parameters are obtained from equation 4.14. R is a regression coefficient.

Temperature (°C)	η_0	G_i	R^2
210	9.46×10^5	9.33	0.9378
230	-9.57×10^5	-5.95	0.9596
250	-63166.01	-94.67	0.9635
270	3.57×10^5	4.39	0.9393
290	1.14×10^5	0.66	0.8795

Table 4.51: Ferry's parameter η_0 and G_i for polypropylene. These parameters are obtained from equation 4.13. R is a regression coefficient.

Temperature (°C)	η_0	G_i	R^2
170	-451.58	-3262.60	0.7426
190	398.68	12415.30	0.3898
210	254.22	-6244.93	0.9988
230	154.22	4268.48	0.5305
250	-9.88	-13135.10	0.8751
270	30.49	1.79×10^{11}	0.2118
290	8.76	31944.60	0.9994

Table 4.52: Ferry's parameter η_0 and G_i for polypropylene. These parameters are obtained from equation 4.14. R is a regression coefficient.

Temperature (°C)	η_0	G_i	R^2
170	2.08×10^5	6.70	0.9086
190	41937.10	16.24	0.8710
210	48444.60	2.02	0.6454
230	1.51×10^5	0.45	0.7628
250	33096.80	1.96	0.7962
270	2564.91	1.40	0.8327
290	-79.22	-10.94	0.3525

Table 4.53: Ferry's parameter η_0 and G_i for amorphous polystyrene. These parameters are obtained from equation 4.13. R is a regression coefficient.

Temperature (°C)	η_0	G_i	R^2
170	5828.85	7576.52	0.9970
190	529.26	7862.23	0.7488
210	50.82	2.82×10^7	0.1445
230	47.46	7.17×10^{10}	0.5730
250	64.33	3744.24	0.9100
270	62.55	1701.11	0.9936
290	33.6	787.72	0.9542

Table 4.54: Ferry's parameter η_0 and G_i for amorphous polystyrene. These parameters are obtained from equation 4.14. R is a regression coefficient.

Temperature (°C)	η_0	G_i	R^2
170	5626.38	8228.79	0.9430
190	27.48	-8250.30	0.7548
210	1.47	-875.15	0.7348
230	-2.57	-841.13	0.5989
250	78.12	17.77	0.8265
270	70.34	117.16	0.9705
290	37.04	479.47	0.7349

Table 4.55: Ferry's parameter η_0 and G_i for crystalline polystyrene. These parameters are obtained from equation 4.13. R is a regression coefficient.

Temperature (°C)	η_0	G_i	R^2
190	1.69×10^5	51.04	0.4338
210	*	*	*
230	339.20	1.36×10^{14}	0.3574
250	139.32	6.31×10^{12}	0.1821
270	110.09	13891.00	0.6490
290	318.20	685.75	0.8994

Table 4.56: Ferry's parameter η_0 and G_i for crystalline polystyrene. These parameters are obtained from equation 4.14.

Temperature (°C)	η_0	G_i	R^2
190	-704.01	-4436.40	0.9824
210	48.54	0.01	0.3125
230	16408.90	0.57	0.5867
250	32054.00	1.463	0.7403
270	2.04	-2830.60	0.8501
290	117.15	1270.12	0.9254
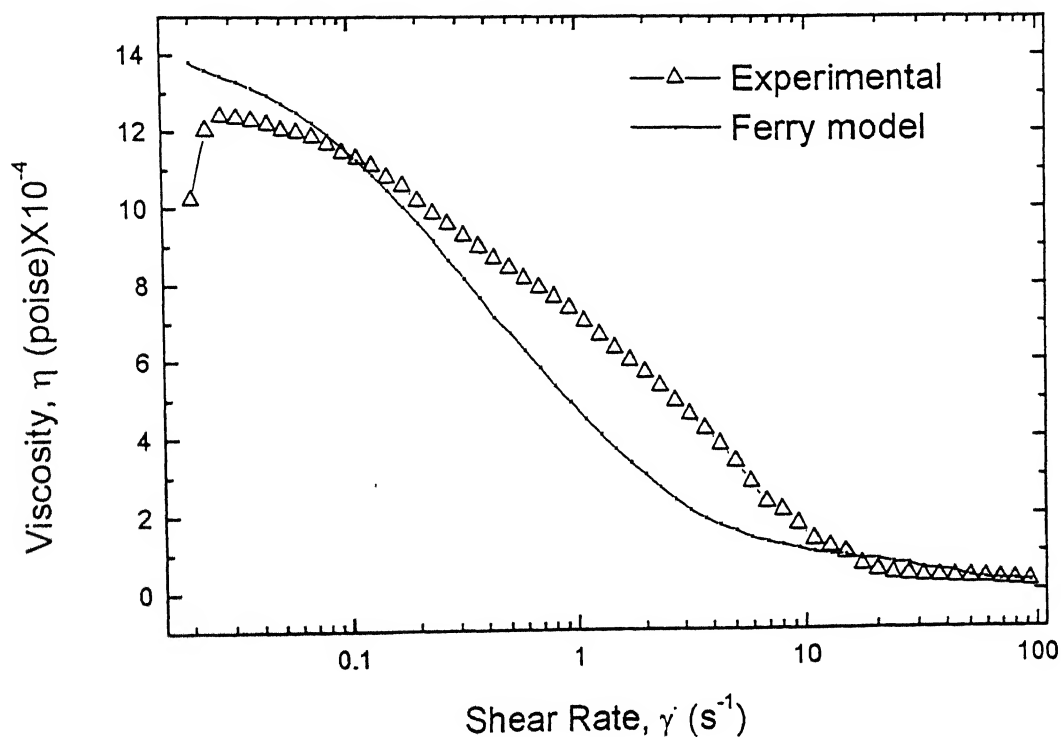
Fig. 4.11 *A representative best fit curve for Ferry's model (crystalline polystyrene at 190^0C).*

Spencer and Dillon's Model (1949) [88-89]: In order to describe the viscosity of polymer melts over a wide range of shear rate, Spencer and Dillon have proposed two empirical relations. This is represented as

$$\eta = \eta_0 \exp\left(-\frac{\tau}{b}\right) \qquad \qquad \ldots(4.15)$$

or

$$\tau = -b \ln\left(\frac{\eta}{\eta_0}\right) \qquad \qquad \ldots(4.16)$$

and

$$\gamma = -\frac{b \ln\left(\dfrac{\eta}{\eta_0}\right)}{\eta} \qquad \qquad \ldots(4.17)$$

where τ, η and γ are the shear stress, viscosity and shear rate respectively. The other fitting parameters b and η_0 are obtained from curve fitting and shown in Tables 4.57-4.64 for low density polyethylene, polypropylene and polystyrene (both amorphous and crystalline). The fitting parameters, b and η_0 gradually decrease with an increase of temperature for both the materials. This model shows a very good fit to the experimental data of shear stress and shear rate data. A representative best fit plot of viscosity versus shear rate for low density polyethylene at 230°C is shown in Figure 4.12.

Table 4.57: Spencer and Dillon's parameter b and η_0 for low density polyethylene. These parameters are obtained from equation 4.16. R is a regression coefficient.

Temperature (°C)	b	η_0	R^2
210	6368.12	26148.10	0.9655
230	5218.51	14177.50	0.9766
250	5408.69	9741.33	0.9797
270	3019.24	4011.93	0.9608
290	537.66	3428.03	0.9499

Table 4.58: Spencer and Dillon's parameter b and η_0 for low density polyethylene. These parameters are obtained from equation 4.17. R is a regression coefficient.

Temperature (°C)	b	η_0	R^2
210	4338.17	1.17×10^5	0.9995
230	5106.68	14155.91	0.9987
250	7089.71	5224.04	0.9960
270	3551.13	2950.14	0.9926
290	335.55	41638.20	0.9909

Table 4.59: Spencer and Dillon's parameter b and η_0 for polypropylene. These parameters are obtained from equation 4.16. R is a regression coefficient.

Temperature (°C)	b	η_0	R^2
170	1924.31	16576.01	0.5276
190	1512.96	14209.70	0.3248
210	5090.18	818.647	0.9523
230	966.49	840.77	0.3961
250	923.43	459.60	0.5786
270	201.42	698.49	0.4646
290	414.71	44.40	1.6555

Table 4.60: Spencer and Dillon's parameter b and η_0 for polypropylene. These parameters are obtained from equation 4.17. R is a regression coefficient.

Temperature (°C)	b	η_0	R^2
170	2677.47	4700.95	0.8941
190	686.18	1.24×10^6	0.9047
210	-683.88	0.44	0.8989
230	-825.37	2.69	0.6687
250	526.16	1941.15	0.9068
270	-87.13	0.02	0.9791
290	615.66	35.09	0.8827

Table 4.61: Spencer and Dillon's parameter b and η_0 for amorphous polystyrene. These parameters are obtained from equation 4.16. R is a regression coefficient.

Temperature (°C)	b	η_0	R^2
170	12673.30	5169.25	0.8220
190	2867.36	2495.30	0.5571
210	724.64	1489.09	0.1055
230	1449.97	110.20	0.1996
250	12.14	89.20	0.6712
270	13.53	90.83	0.9049
290	1226.08	29.14	0.7149

Table 4.62: Spencer and Dillon's parameter b and η_0 for amorphous polystyrene. These parameters are obtained from equation 4.17. R is a regression coefficient.

Temperature (°C)	b	η_0	R^2
170	12414.60	5230.63	0.9200
190	960.69	3.01×10^5	0.7363
210	-366.06	1.16	0.8026
230	167.76	9696.25	0.6075
250	12.20	93.93	0.8177
270	36.96	73.70	0.9677
290	1139.15	29.46	0.8322

Table 4.63: Spencer and Dillon's parameter b and η_0 for crystalline polystyrene. These parameters are obtained from equation 4.16. R is a regression coefficient.

Temperature (°C)	b	η_0	R^2
190	3397.37	41216.70	0.5613
210	623.06	1101.92	0.2730
230	379.61	1433.81	0.0692
250	1166.94	1172.28	0.2656
270	2699.14	319.87	0.8127
290	2053.46	228.86	08984

Table 4.64: Spencer and Dillon's parameter b and η_0 for crystalline polystyrene. These parameters are obtained from equation 4.17. R is a regression coefficient.

Temperature (°C)	b	η_0	R^2
190	5310.92	5468.78	0.9635
210	-218.80	0.70	0.8425
230	-193.16	0.17	0.7906
250	-337.10	0.07	0.9256
270	399.26	38221.60	0.8133
290	2822.71	98.91	0.9339
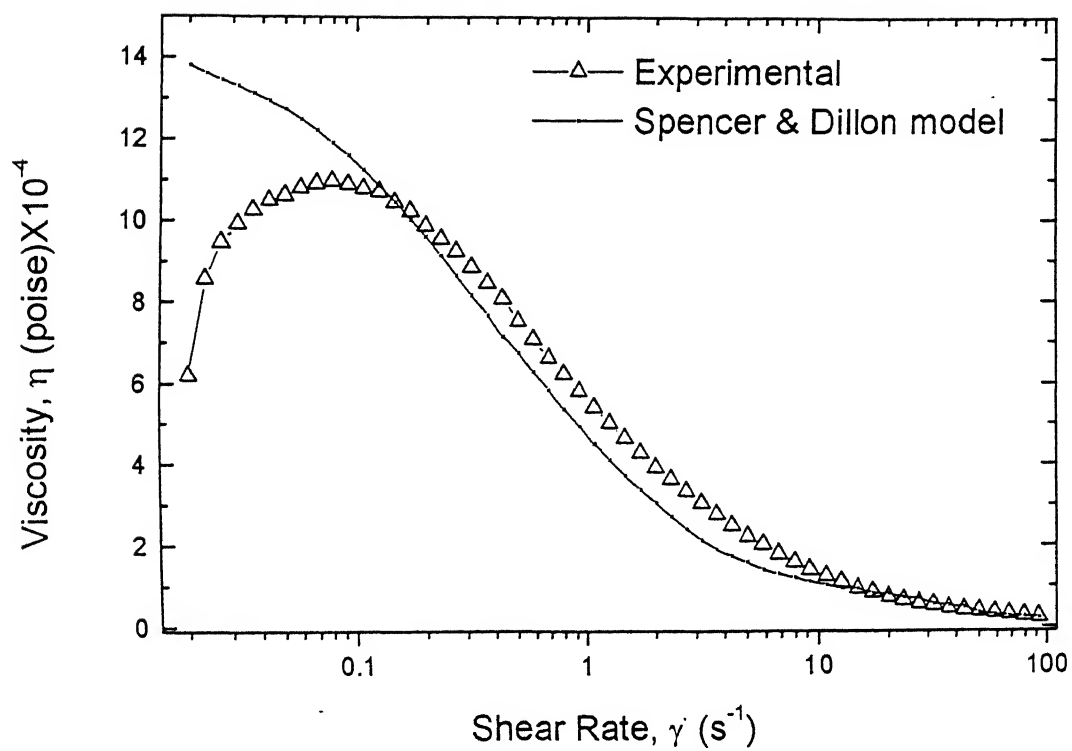
Fig. 4.12 *A representative best fit curve for Spencer and Dillon's model (low density polyethylene at 230°C).*

Berger's Model (1998): Another four parameter model has been developed by Berger to fit the experimental data of shear stress versus shear rate over a wide range of shear rate. This is represented as

$$\tau = C_1 + C_2 \left[1 - \exp\left(-\frac{\gamma}{C_3} \right) \right] + \frac{\gamma}{C_4} \qquad \ldots.(4.18)$$

where τ, γ are shear stress and shear rate respectively. The other parameters are obtained from curve fitting and given in Tables 4.65-4.68 for low density polyethylene, polypropylene and polystyrene (both amorphous and crystalline) respectively. The fitting parameters, C_1 and C_2 gradually decreases with increasing temperature for low density polyethylene but the other fitting parameters, C_3 and C_4 change independently with temperature. This Berger's model shows a better fit to the experimental data of shear stress and shear rate compared with Bingham and Herschel-Bulkley models. A representative best fit plot of shear stress versus shear rate for low density polyethylene at 230°C is shown in Figure 4.13.

Table 4.65: Berger's parameter C_1, C_2, C_3 and C_4 for low density polyethylene. These are obtained from equation 4.18. R is a regression regression coefficient.

Temperature (°C)	C_1	C_2	C_3	C_4	R^2
210	1078.97	16905.10	2.10	0.01	0.9922
230	604.96	11604.20	2.04	0.01	0.9951
250	721.07	9505.36	2.86	0.007	0.9897
270	522.15	5478.75	5.29	0.015	0.9851
290	156.69	1416.62	2.16	0.07	0.9652

Table 4.66: Berger's parameter C_1, C_2, C_3 and C_4 for polypropylene. These are obtained from equation 4.18. R is regression coefficient.

Temperature (°C)	C_1	C_2	C_3	C_4	R^2
170	-120.98	6580.23	1.57	0.02	0.9327
190	-93.11	7253.46	3.17	6315.46	0.9112
210	-8.98	2891.15	3.65	0.01	0.9998
230	-81.59	2576.84	3.74	0.00	0.8970
250	-52.44	1851.98	4.28	0.72	0.9411
270	-7.48	743.57	3.01	0.00	0.9136
290	0.28	190.84	61.82	0.18	0.9994

Table 4.67: Berger's parameter C_1, C_2, C_3 and C_4 for amorphous polystyrene. These are obtained from equation 4.18. R is regression coefficient.

Temperature (°C)	C_1	C_2	C_3	C_4	R^2
170	-140.00	5199.07	1.05	0.001	0.9991
190	-160.35	4827.87	2.33	0.01	0.8781
210	-97.38	3204.81	7.48	5.04×10^{35}	0.8649
230	-55.70	2394.94	17.99	1744.65	0.9375
250	60.82	12.53	78.98	-1.98	0.8105
270	0.83	655000	-1.57×10^7	0.02	0.9683
290	-7.39	1284.66	45.22	16.70	0.9909

Table 4.68: Berger's parameter C_1, C_2, C_3 and C_4 for crystalline polystyrene. These are obtained from equation 4.18. R is regression coefficient.

Temperature (°C)	C_1	C_2	C_3	C_4	R^2
190	-156.71	13858.40	1.18	0.03	0.9218
210	-140.50	10594.01	3.98	4.89×10^{14}	0.9723
230	-115.00	6720.23	2.80	2.01×10^{10}	0.9095
250	-65.16	3836.50	5.28	7.83×10^{11}	0.8616
270	-22.43	4273.88	16.67	600.74	0.9843
290	-21.01	3613.57	25.37	17244.10	0.9916
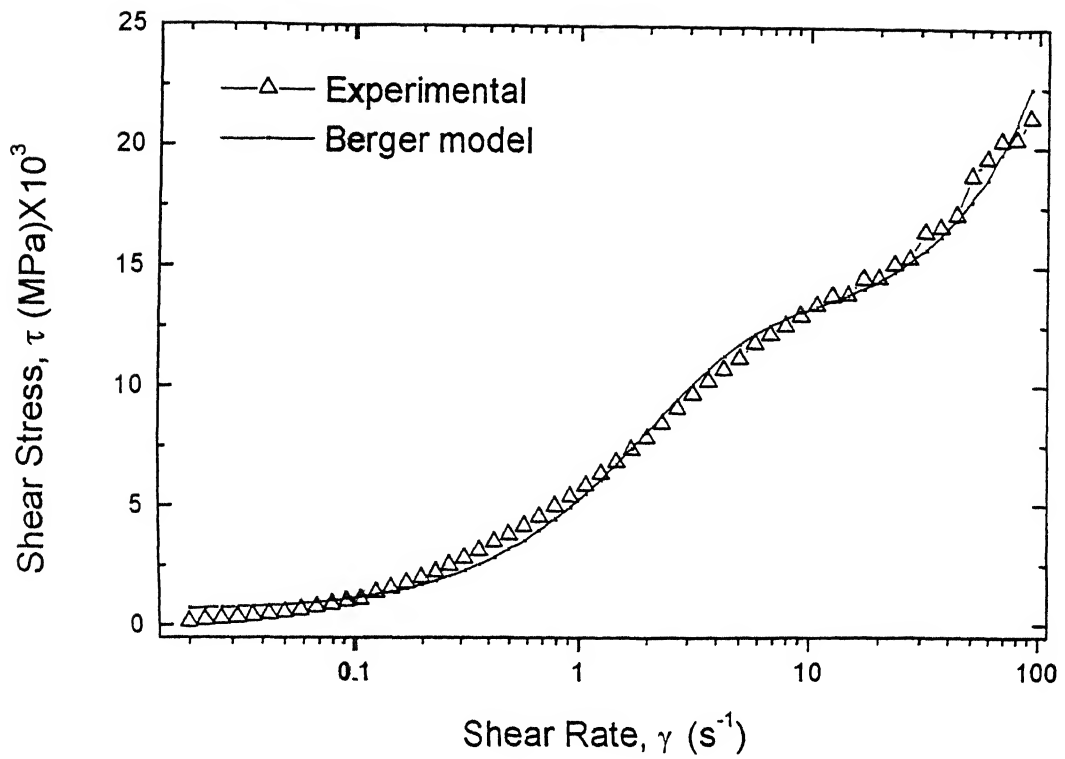
Fig. 4.13 *A representative best fit curve for Berger's model (low density polyethylene at 230°C).*

4.2 Testing Of Proposed Model:

The result of proposed modeling efforts is a fully three dimensional variable based constitutive model of polymer network theory in which glass transition temperature, relaxation time and limiting network extensibilities properties are needed to be completely characterized for the die swell phenomenon of polymer over a range of shear rate (0.02 to 100 s⁻¹) and temperature (170 to 290°C). The quantitative prediction of die swell using equation (3.79) would involve the measurement of first normal stress difference, shear stress, shift factor, relaxation time, radius of die and average velocity of fluid through die. For convenience, the shift factor is calculated from equation (3.58).

First normal stress difference and shear stress were measured by advanced rheometric expansion system over a range of temperature (170 to 290°C) and shear rate (0.02 to 100 s⁻¹). For low density polyethylene, polypropylene and polystyrene (both amorphous and crystalline) to find out the correlation between them.

Figures 4.14-4.17 shows the representative plots of the ratio of first normal stress difference to shear stress against shear rate for low density polyethylene at 250°C, polypropylene at 250°C, amorphous polystyrene at 190°C and crystalline polystyrene at 230°C respectively. It indicates that the ratio of first normal stress difference to shear stress is a strong function of shear rate. Similar trends in the ratio of first normal stress difference to shear stress and shear rate relationship on temperature are also observed for low density polyethylene, polypropylene, amorphous polystyrene and crystalline polystyrene (not shown here). Hence power law relationship describing the data mentioned above is given below as obtained from the regression analysis

$$\frac{N_1}{\tau} = A\left(\gamma\right)^n \qquad \qquad ....(4.19)$$

85

where N_1, τ_w and γ are the first normal stress difference, shear stress and shear rate respectively. A and n are model parameters. These are tabulated in Table 4.69.

Table 4.69: Model parameters

Parameter	Low density polyethylene at 250°C	Polypropylene at 250°C	Amorphous polystyrene at 190°C	Crystalline polystyrene at 230°C
A	2.29	0.52	0.55	0.31
n	0.30	0.39	0.51	0.54
R^2	0.8095	0.8843	0.9405	0.9431
A_1	-3.21	-1.60	-5.48	-0.05
B_1	5.59	2.10	5.27	0.35
n_1	0.16	0.16	0.15	0.51
R_1^2	0.9472	0.9971	0.9991	0.9851

It is interesting to note that both model parameters A and n depend on material. But the regression coefficient varies from 0.8095 to 0.9431.

In this study an attempt was made to characterize the ratio of first normal stress difference to shear stress and shear rate in a better way by a three parameter power law model. A relationship obtained through regression analysis is give below

$$\frac{N_1}{\tau} = A_1 + B_1 \left(\gamma \right)^{n_1} \qquad \qquad ....(4.20)$$

where N_1, τ_w and γ are first normal stress difference, shear stress and shear rate respectively. And A_1, B_1 and n_1 are model parameters. These model parameters are also included in Table 4.69. An interesting point in this study is that the value of material constant A_1 is negative for the polymers studied. The reason for the negative value of A_1 is not clear at this time.

86
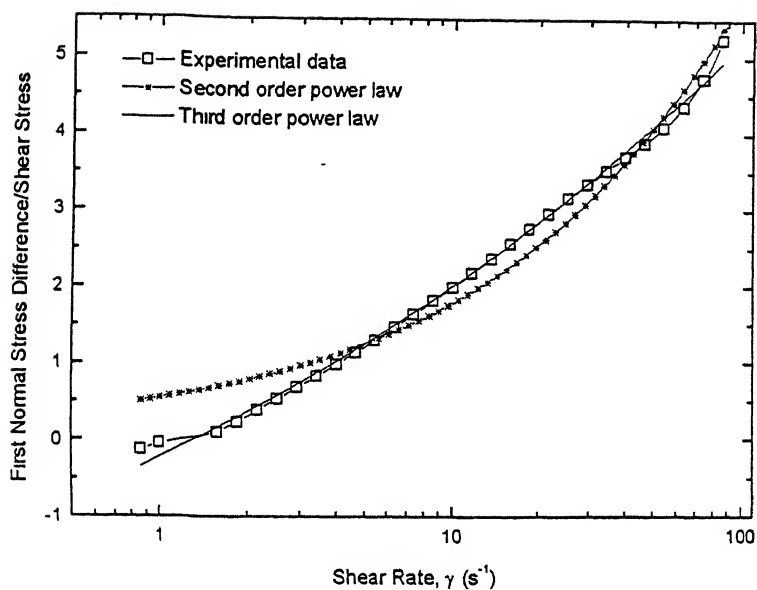
**Fig. 4.16** *First normal stress difference/shear stress versus shear rate for amorphous polystyrene at a temperature of 190°C.*
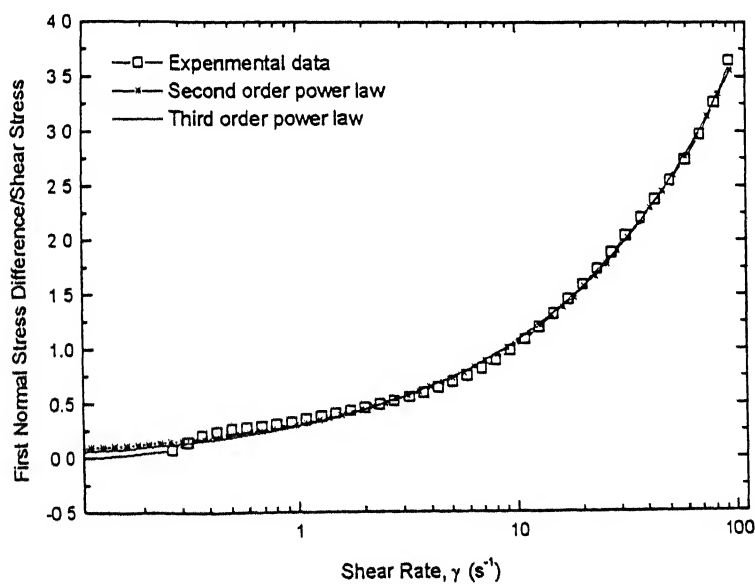
Fig. 4.17 *First normal stress difference/shear stress versus shear rate for crystalline polystyrene at a temperature of 230°C.*

88

4.2.1 Effect of Shear Rate and Relaxation Time on Die Swell:

The die swell of polymer depends on the shear rate and relaxation time. To understand the variation of extrudate swell with shear rate and relaxation time, polypropylene, low density polyethylene and polystyrene (both amorphous and crystalline) have been investigated. The die swell is calculated at the desired shear rate for polypropylene, low density polyethylene and polystyrene (both amorphous and crystalline) using equation (3.79). Here die radius of $1X10^{-3}$ m, average velocity of $1X10^{-3}$ m/s, glass transition temperature of -80°C, c_1 of 16.35 and c_2 of 52.50 are used to compute these die swell data for polystyrene. Representative plot of die swell versus shear rate of polypropylene at different relaxation times is shown in Figure 4.18. The results indicate that the die swell of polypropylene increases in a progressive manner with relaxation time at a fixed shear rate. Bur the change is not marginal, when the relaxation time is changed from 0.1 to 1 s. The change is noticeable at 10 s^{-1} shear rate for 0.1 s relaxation time. At high shear rate (30 s^{-1} and above) a sharp increase in die swell is observed for 0.1 s and 1 s relaxation times. A noticeable increase in die swell is observed from low shear rate to high shear rate at 100 s relaxation time. For example at a temperature of 290°C using the glass transition temperature of -80°C, radius of die $1X10^{-3}$ m, average velocity of $1X10^{-3}$ m/s, c_1 of 16.35 and c_2 of 52.50 the equilibrium die swell of polypropylene increases by about 0.01, 0.02, 0.03 and 0.06 factors with increasing shear rate from 0.02 to 93 s^{-1} for 0.1, 1, 10 and 100 s relaxation time respectively. But at a fixed shear rate of 93 s^{-1}, the equilibrium die swell increases by about 0.002, 0.017 and 0.044 factors when the relaxation time changes from 0.1 to 1, 10, and 100 s respectively. Similar trends are also observed for other polymers (low density polyethylene, polypropylene, amorphous polystyrene and crystalline polystyrene).

The increase in die swell with increasing shear rate may be attributed to the considerable increase in the recoverable elastic energy of the system at higher shear rates (Arai and Aoyama 1963 [90]). But the higher die swell at higher relaxation time may be due to the low rate of stress relaxation.
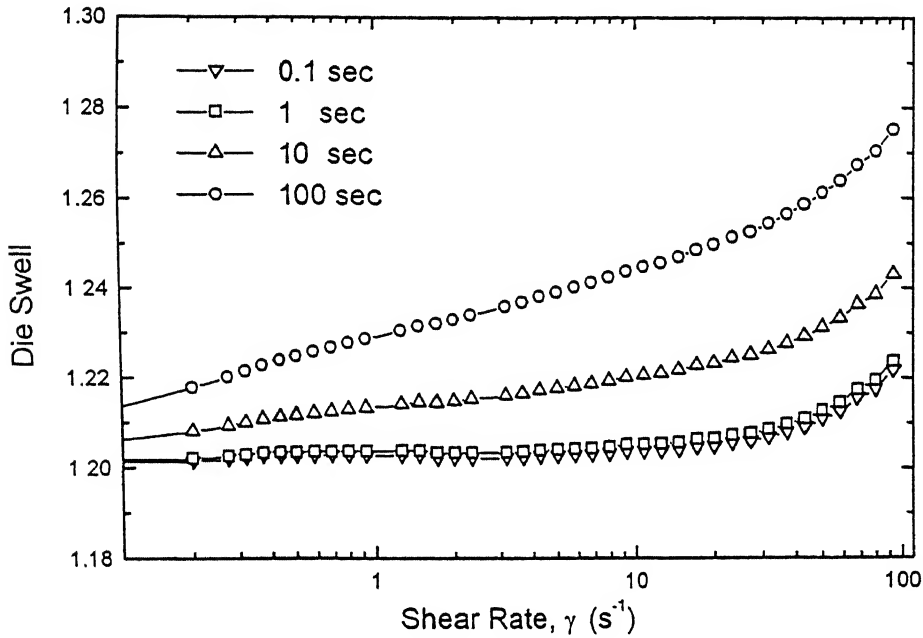

Fig. 4.18 *Die swell versus shear rate for polypropylene at 290°C for different relaxation times (die radius = 1X10^{-3} m, average velocity = 1X10^{-3} m/s, glass transition temperature = -80°C, c_1 = 16.35 and c_2 = 52.5).*

4.2.2 Effect of Shear Rate and Temperature on Die Swell:

This section discusses how the variations of shear rates influence the die swell behaviour of polymer over a range of temperature. Temperature of 170, 190, 210, 250 and 290°C are used for this investigation. The die swell is calculated at the desired shear rate and temperature for low density polyethylene, polypropylene and polystyrene (both amorphous and crystalline) using equation (3.79) and experimental data of first normal stress difference and shear stress. Same parameters (die radius of $1X10^{-3}$ m, average velocity of $1X10^{-3}$ m/s, glass transition temperature of -80°C, c_1 of 16.35 and c_2 of 52.5) for calculation of the die swell used in previous section are also treated here. Representative plot of die swell versus shear rate for polypropylene at different temperatures is shown in Figure 4.19. This shows the expected behaviour of the dependence of die swell on shear rate (die swell increases with increasing shear rate). It may be due to the considerable increase in the recoverable elastic energy of the system with shear rate. However the increased temperature, the die swell decreases at each shear rate. At high temperature the change of die swell is marginal. It is well known that an increase in the temperature of polymer melts: increases the chain mobility resulting in reduced capacity of polymer molecules to store the deformation energy; and hence there is a reduction of die swell values. This is also explained by the faster relaxation of molecular orientation at elevated temperature. For example at a shear rate of 93 s^{-1} using the glass transition temperature of -80°C, radius of die of $1X10^{-3}$ m, average velocity of $1X10^{-3}$ m/s, c_1 of 16.35 and c_2 of 52.5, the equilibrium die swell of polypropylene decreases by about 0.98, 0.94, 0.86 and 0.81 factors on additions of 20, 40, 80 and 120°C to the base temperature of 170°C respectively. But at a very low shear rate (0.2 s^{-1}) the change if die swell with temperature is very small. Similar trends are also observed for low density

91

polyethylene, crystalline polystyrene and amorphous polystyrene (not shown here).
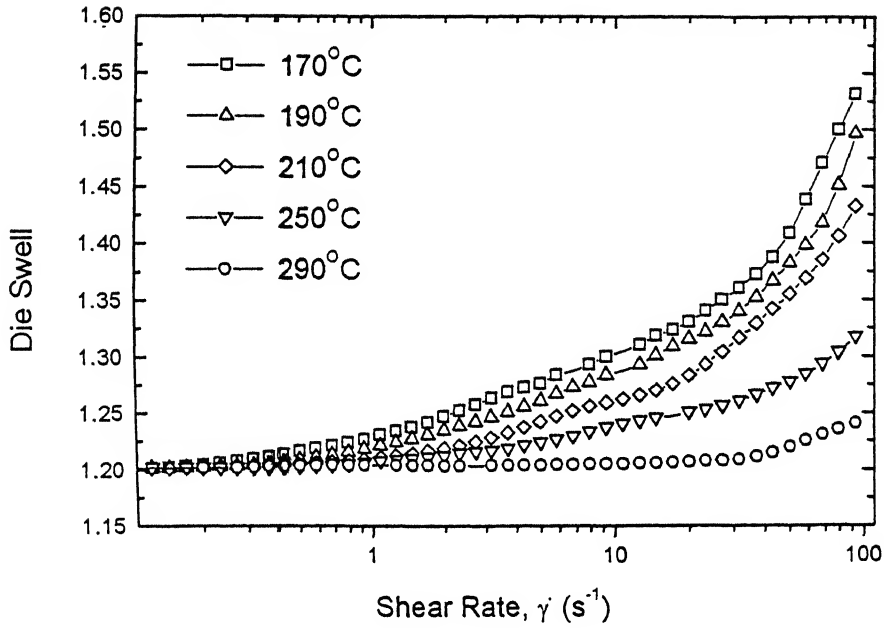
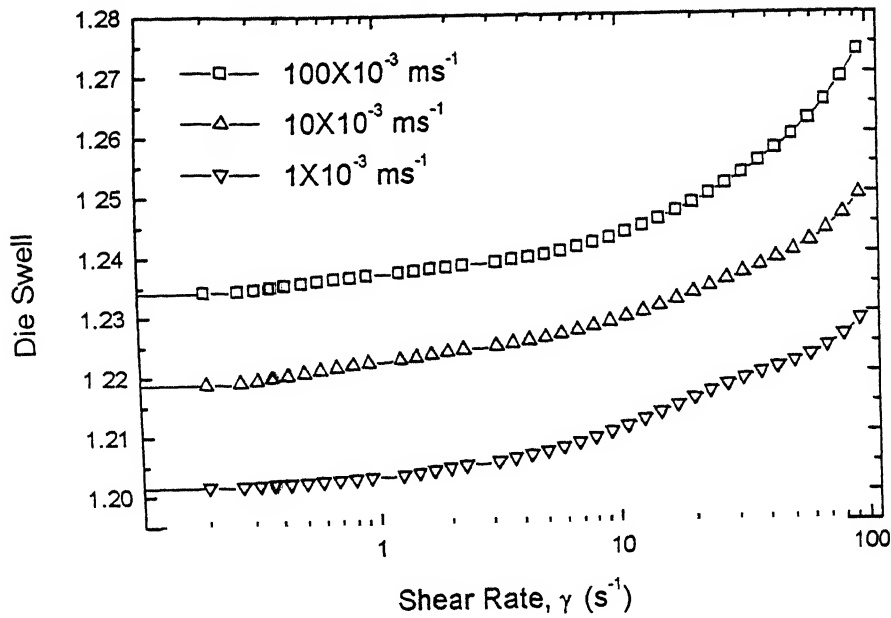
Fig. 4.19 *The effect of shear rate and temperature on die swell for polypropylene (die radius = $1X10^{-3}$ m, average velocity = $1X10^{-3}$ m/s, glass transition temperature = -80°C, relaxation time = 1 s, c_1 = 16.35 and c_2 = 52.5).*

4.2.3 Effect of Shear Rate and Average Fluid Velocity on Die Swell:

In order to understand the effect of fluid velocity on die swell, experimental measurement of first normal stress difference and shear stress and numerical values of die swell are carried out on low density polyethylene, polypropylene and polystyrene over a range of shear rate, temperature, die radius and relaxation time. The numerical values of die swell are calculated from the proposed model equation (3.79) and using same parameters (die radius of 1×10^{-3} m, relaxation time of 1 s, glass transition temperature of $-80^{\circ}C$, c_1 of 16.35 and c_2 of 52.5). A representative plot of die swell versus shear rate at different fluid velocity is shown in Figure 4.20 for polypropylene at a temperature of 290°C. Similar trend means the increased die swell with increasing shear rate is also observed here. In addition to this observation, the die swell increases in a progressive manner with fluid velocity at each shear rate. The observed value of die swell at high fluid velocity is attributed to the low rate of stress relaxation. Neilsen [91] has also pointed out the important effect on die swell of the time for the polymer to flow through the capillary. The shorter the time that polymer spends in the die due to higher velocity, the greater is the die swell (Rogers 1970 [92], Neilsen 1977 [91] and Minagawa and White 1976 [93]). For example at a temperature of 290°C and shear rate of 0.02 s^{-1} glass transition temperature of $-80°C$, radius of die of 1×10^{-3} m, c_1 of 16.35, c_2 of 52.5 and relaxation time of 1 s, the equilibrium die swell of polypropylene increases by about 0.01 and 0.03 factors with increasing average velocity of fluid from 1×10^{-3} to 10×10^{-3} m/s and 1×10^{-3} to 100×10^{-3} m/s respectively. But at higher shear rate of 93 s^{-1} the die swell increases by 0.02 and 0.04 factors for the corresponding ratio of die of 1×10^{-3} m, c_1 of 16.35, c_2 of 52.5 and relaxation time of 1 s.

Similar trends are also observed for other polymers (low density polyethylene, amorphous polystyrene and crystalline polystyrene) and variables (temperature, die geometry, relaxation time, etc.).
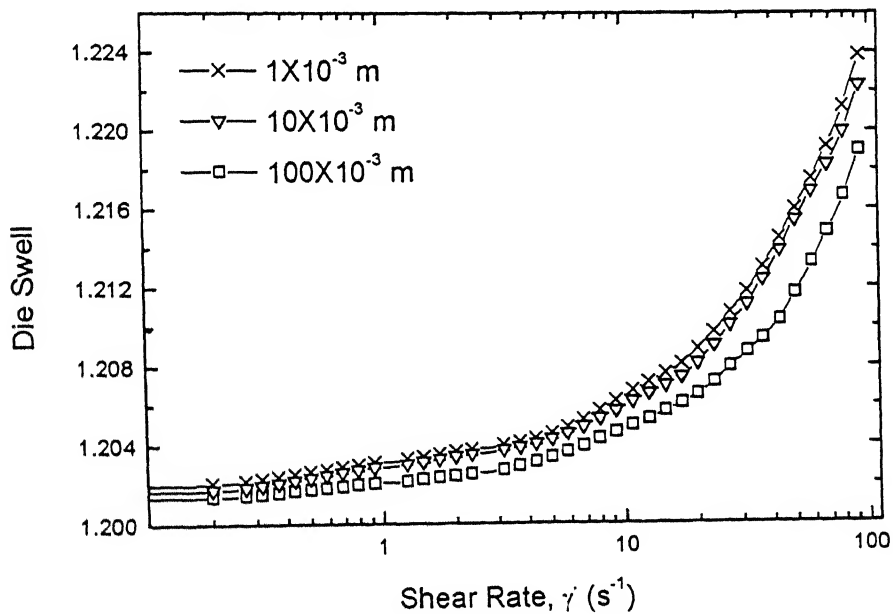

Fig. 4.20 *Die swell versus shear rate at different fluid velocity for polypropylene at 290°C (die radius = $1X10^{-3}$ m, glass transition temperature = -80°C, relaxation time = 1 s, c_1 = 16.35 and c_2 = 52.5).*

4.2.4 Effect of Shear Rate and Die Radius on Die Swell:

This section discusses how the variations of shear rate and die radius influence the die swell behaviour of low density polyethylene, polypropylene and polystyrene over a range of shear rate, temperature, relaxation time, etc. Die radius of $1X10^{-3}$, $10X10^{-3}$ and $100X10^{-3}$ m are used for this investigation. The numerical value of die swell is obtained from equation (3.79) using same other parameters (average velocity of $1X10^{-3}$ m/s, relaxation time of 1 s, glass transition temperature of -80°C, c_1 of 16.35 and c_2 of 52.5). A representative

94

plot of die swell versus shear rate at 1×10^{-3}, 10×10^{-3} and 100×10^{-3} m die radius for polypropylene is shown in Figure 4.21. Here temperature is 290°C. Similar trend of increased die swell with shear rate is observed here. In addition to this observation, die swell decreases with an increase of die radius from 1×10^{-3} and 10×10^{-3} m to die radius of 100×10^{-3} m at each shear rate. But there is very small change in die swell for the die radius of 1×10^{-3} and 10×10^{-3} m. The reason for this decrease of die swell may be due to the molecular orientation in the flow is the result of the extensional flow in the entrance region of the die and not as a result of shear deformation within the die. Similar trend is also observed for other polymers and other processing conditions (not shown here).

Fig. 4.21 *Die swell versus shear rate at different die radius for polypropylene at 290°C (average velocity = 1×10^{-3} m/s, relaxation time = 1 s, glass transition temperature = -80°C, $c_1 = 16.35$ and $c_2 = 52.5$).*

4.3 Comparison of Proposed Model With Existing Models:

The die swell at different temperatures (170 to 290°C), shear rates (0.02 to 100 s^{-1}) and ratio of first normal stress difference to shear stress (0 to 10) have been computed for low density polyethylene, polypropylene, amorphous polystyrene and crystalline polystyrene using equation (3.79). Die radius of $1X10^{-3}$ m, average velocity of $1X10^{-3}$ m/s, relaxation time of 1 s, c_1 of 16.35 and c_2 of 52.5 are used for this calculation. The results of die swell are plotted against the ratio of first normal stress difference to shear stress and shear rate. Representative plots of die swell versus the ratio of first normal stress difference to shear stress for low density polyethylene at 250°C, polypropylene at 250°C, amorphous polystyrene at 190°C and crystalline polystyrene at 230°C are shown in Figures 4.22 to 4.25 respectively. Similarly, representative plots of die swell versus shear rate for polypropylene at 250°C, amorphous polystyrene at 190°C, crystalline polystyrene at 230°C and low density polyethylene at 250°C are shown in Figures 4.26 to 4.29 respectively. It is interesting to note that the die swell increases with an increase of the ratio of first normal stress difference to shear stress and shear rate for all the systems. This may be attributed to the considerable increase in the recoverable elastic energy of the systems at high shear rates (Arai and Aoyama 1963 [90]).

The die swell is also calculated using Tanner [12] [equation (1.8)], Bagley [8] [equation (1.9)], White and Roman [11] [equation (1.12)], Macosko [48] [equation (1.14)] and Kumar et al. [49] [equation (1.15)]. These calculated values are compared with the proposed model in the same Figures 4.22 to 4.29.

Proposed model shows good agreement with Macosko model, but divergence is observed in all other models like White and Roman, Tanner, Kumar and Gupta and Bagley (Figure 4.22 to 4.29).

Now to compare the validity of proposed model (Equation 3.79) and existing models like Tanner's model [12] [equation (1.8)], Bagley's model [8] [equation (1.9)], White and Roman's model [11] [equation (1.12)], Macosko's model [48] [equation (1.14) and Kumar et al. [49] [equation (1.15)] with the experimental data, the experimental values of die swell for low density polyethylene at 250°C are plotted against shear rate in Fig 4.29 the theoretical values calculated from proposed model equation (3.79) and Macosko model [48] [equation (1.14)] are in good accordance with the experimental values (within $\pm 1\%$) after a shear rate of 1.15 s^{-1}. But divergence is observed in all other model. The proposed model equation also reveals that the degree of dependence of shear rate, ratio of first normal stress difference to shear stress, relaxation time, radius of die and fluid velocity is a highly non linear function.
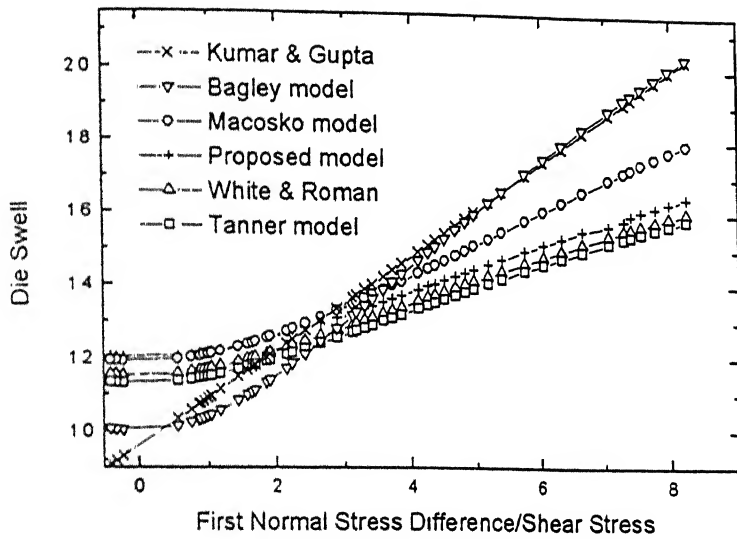
Fig. 4.22 *Die swell versus first normal stress difference/shear stress for proposed model (eq. 3.79) and existing models i.e. Tanner (eq. 1.8), Bagley (eq. 1.9), White and Roman (eq. 1.12), Macosko (eq. 1.14) and Kumar and Gupta (eq. 1.15) at 250°C for low density polyethylene.*
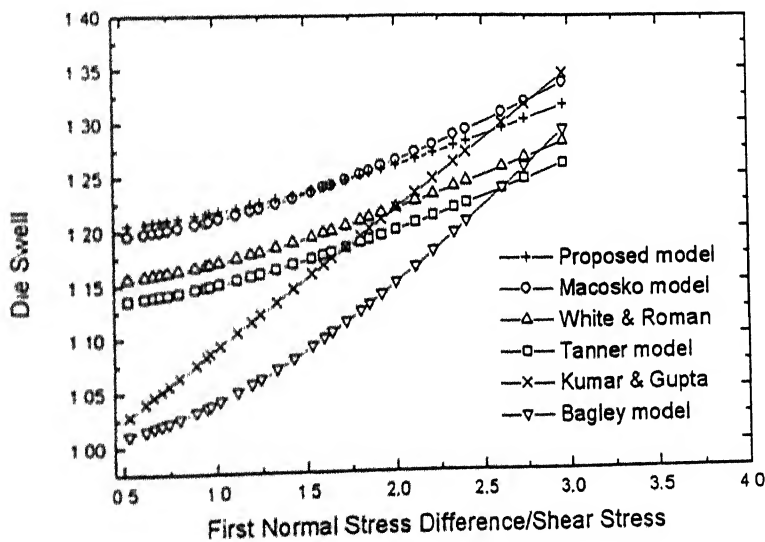

Fig. 4.23 *Die swell versus first normal stress difference/shear stress for proposed model (eq. 3.79) and existing models i.e. Tanner (eq. 1.8), Bagley (eq. 1.9), White and Roman (eq. 1.12), Macosko (eq. 1.14) and Kumar and Gupta (eq. 1.15) at 250°C for polypropylene.*

98

Fig. 4.24 *Die swell versus first normal stress difference/shear stress for proposed model (eq. 3.79) and existing models i.e. Tanner (eq. 1.8), Bagley (eq. 1.9), White and Roman (eq. 1.12), Macosko (eq. 1.14) and Kumar and Gupta (eq. 1.15) at 190°C for amorphous polystyrene.*

Fig. 4.25 *Die swell versus first normal stress difference/shear stress for proposed model (eq. 3.79) and existing models i.e. Tanner (eq. 1.8), Bagley (eq. 1.9), White and Roman (eq. 1.12), Macosko (eq. 1.14) and Kumar and Gupta (eq. 1.15) at 230°C for crystalline polystyrene.*

99

Fig. 4.26 *Die swell versus shear rate for proposed model (eq.3.79) and existing models i.e. Tanner (eq. 1.8), Bagley (eq. 1.9), White and Roman (eq. 1.12), Macosko (eq. 1.14) and Kumar and Gupta (eq. 1.15) at 250°C for polypropylene.*
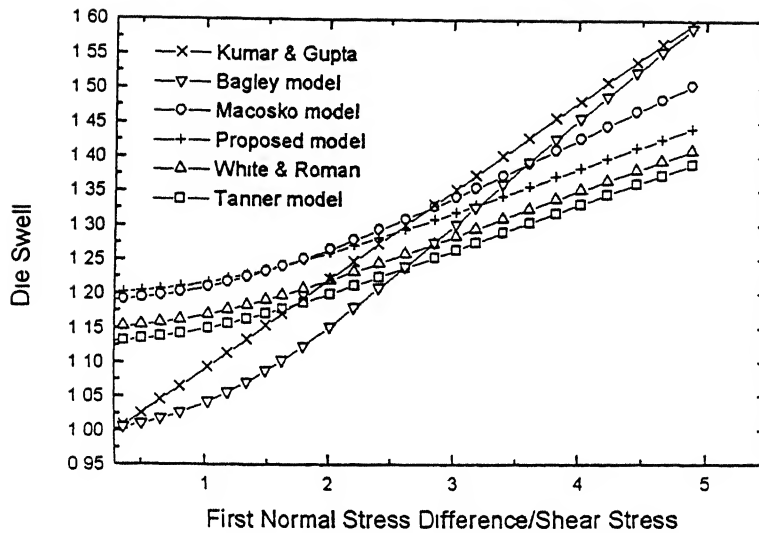

Fig. 4.27 *Die swell versus shear rate for proposed model (eq. 3.79) and existing models i.e. Tanner (eq. 1.8), Bagley (eq. 1.9), White and Roman (eq. 1.12), Macosko(eq. 1.14) and Kumar and Gupta (eq. 1.15) at 190°C for amorphous polystyrene.*
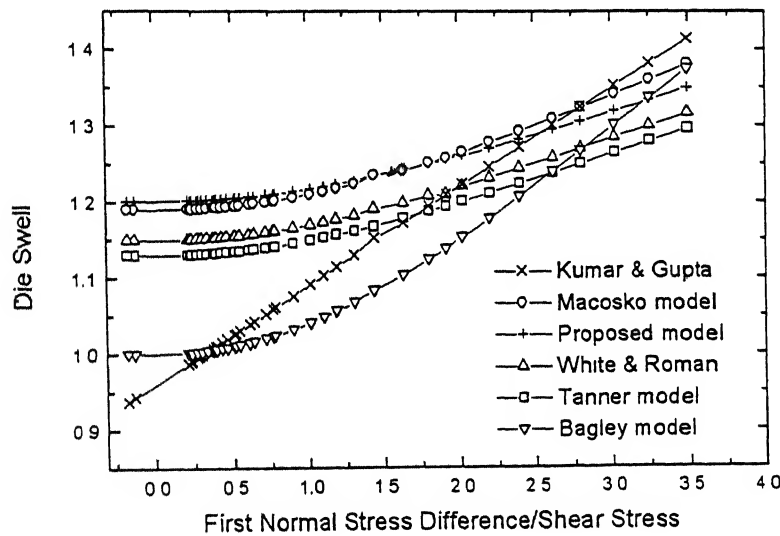
100

Fig. 4.28 *Die swell versus shear rate for proposed model (eq. 3.79) and existing models i.e. Tanner (eq. 1.8) , Bagley (eq. 1.9), White and Roman (eq. 1.12), Macosko (eq. 1.14) and Kumar and Gupta (eq. 1.15) at 230°C for crystalline polystyrene.*
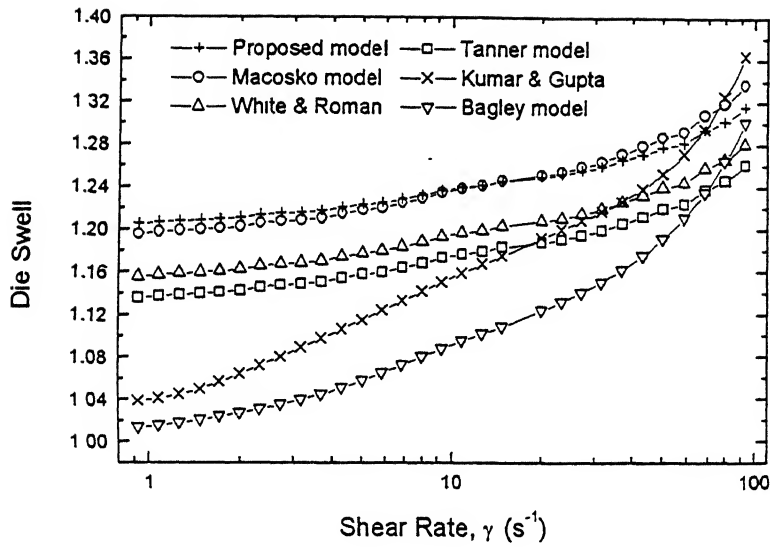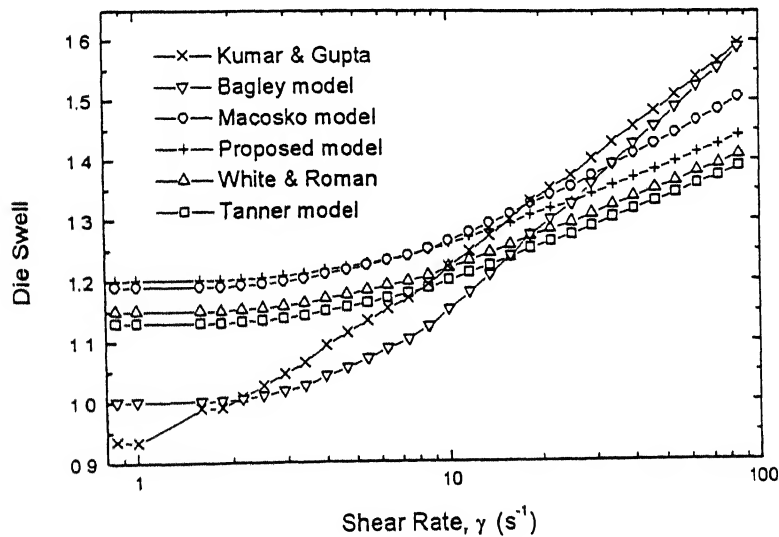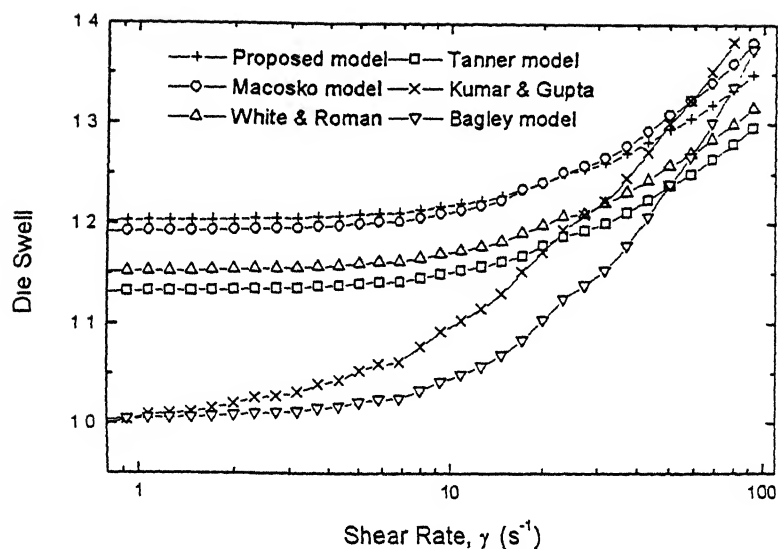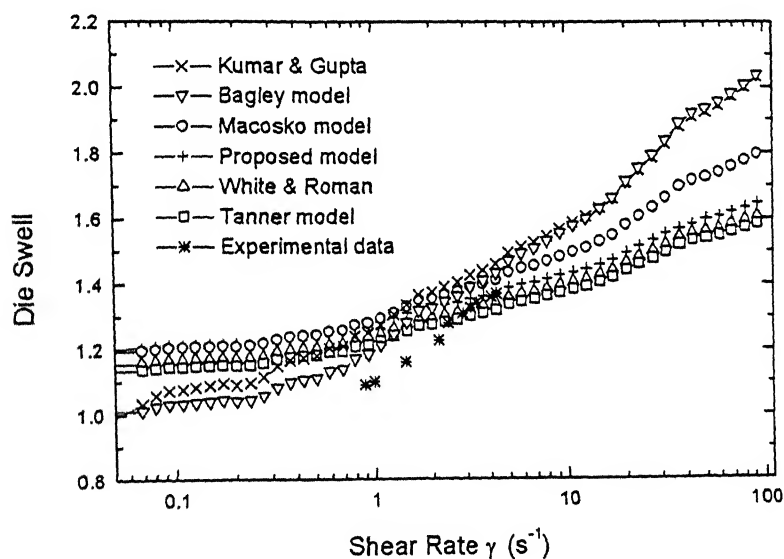

Fig. 4.29 *Die swell versus shear rate for proposed model (eq. 3.79) and existing models i.e. Tanner (eq. 1.8), Bagley (eq. 1.9), White and Roman (eq. 1.12), Macosko (eq. 1.14) and Kumar and Gupta (eq. 1.15) at 250°C for low density polyethylene.*

CHAPTER 5
SUMMARY AND CONCLUSIONS

Rheological properties like viscosity, shear stress, first normal stress difference, etc. of low density polyethylene, polypropylene and polystyrene (both amorphous and crystalline) have been measured by Advanced rheometric expansion system in a parallel plate-plate configuration under steady shear condition over a range of shear rate and processing of temperatures. Similarly die swell measurements are carried out in Randcastle microtruder over a range of shear rate and processing temperature. The following conclusions have been made from the present investigation.

➢ Viscosity of low density polyethylene, polypropylene and polystyrene both amorphous and crystalline decreases with an increase of shear rate in steady shear condition.

➢ But an increased in shear rate increases the first normal stress difference and shear stress of the polymers.

➢ The viscosity versus shear rate plot is analyzed with the help of Power law (1925), Bueche (1962), Cross (1965), Ellis (1977), Carreau (1979), Bingham (1922), Herschel and Bulkley (1926), Casson (1959), Ferry (1942), Spencer and Dillon (1949) and Berger's (1998) model. Bueche, Cross, Ellis, and Carreau model showed good agreement with experimental data.

➢ Die swell of these polymers increases with an increase of shear rates, relaxation time of materials and average velocity of fluid through die.

➢ An increased in polymer melt temperature and die radius decreases the die swell of polymers.

➢ Die swell of low density polyethylene, polypropylene and polystyrene both amorphous and crystalline has been quantified by using first normal stress difference, shear stress, relaxation time, glass transition temperature and other materials parameters. The model equation (3.79) has been tested for different processing scenarios and materials properties such as varying shear rate, temperature, relaxation time, nature of polymers and average velocity of fluids. The experimental data are in good accord with the theoretical predictions of the proposed model and Macosko model. A wide deviation is observed between experimental and all other previously reported models tested.

REFERENCES

(1) J.M. Dealy, and K.F. Wissbrun, *"Melt Rheology and Role in Plastics Processesing,"* Van Nostrand Reinhold, New York, pp. 332 (1989).

(2) A. Garcia-Rajon, and J.M. Dealy, *Polym. Eng. Sci.*, **22**, 158 (1982).

(3) S. Middleman, *"Fundamental of Polymer Processing,"* Mc. GrawHill Book Company, New York, pp. 464 (1977).

(4) A.B. Metzner, W.T. Houghten, R.A. Sailor, and J.L. White, *Trans. Soc. Rheol.*, **5**, 133 (1967).

(5) R.B. Bird, R.K. Prudhomme, and M. Gottlieb, *"Extrudate Swell as Analyzed by Macroscopic Balances,"* The University of Wisconsin, Rheology Research Center Report RRC-35, (1975).

(6) B. Whipple, *"Velocity Distributions in Die Swell,"* Ph.D. dissertation, Washington University, St. Louis, MI, (1974).

(7) W.W. Graessley, S.D. Glasscock, and R.L. Crawley, *Trans. Soc. Rheol.*, **14**, 519 (1970).

(8) E.B. Bagley, and H.J. Duffy, *Trans. Soc. Rheol.*, **14** (4), 545 (1970).

(9) K. Funatsu, and Y. Mori, *Kobunshi Kagaku.*, **29**, 638 (1972).

(10) R.I. Tanner, *J. Polym. Sci.*, Part A-2, **8**, 2067 (1970).

(11) J.L. White, and J.F. Roman, *J. Appl. Polym. Sci.*, **20**, 1005 (1976).

(12) D. Huang, and J.L. White, *Polym. Eng. Sci.*, **19**, 609 (1979).

(13) R. Racin, and D.C. Bogue, *J. Rheology*, **23** (3), 263 (1979).

(14) N. Nakajima, and M. Shida, *Trans. Soc. Rheol.*, **10**, 299 (1966).

(15) J. Vlachopoulos, M.Horie, and S. Lidorikis, *Trans. Soc. Rheol.*, **14**, 519 (1970).

(16) L.A. Utracki, Z. Bakerdjian, and M.R. Kamal, *J. Appl. Polym. Sci.*, **19**, 481 (1975).

(17) F.N. Congswell, *Polym. Eng. Sci.*, **12**, 64 (1972).

(18) A.B. Metzner, and A.P. Metzner, *Rheol. Acta*, **9**, 174 (1970).

(19) J.L. Duda, and J.S. Vrentas, *Can. J. Chem. Eng.*, **50**, 671 (1972).

(20) S. Richardson, *Rheol. Acta*, **9**, 193 (1970).

(21) R.L. Cero, and S. Whitaker, *Chem. Eng. Sci.*, **26**, 785 (1971).

(22) H.B. Phuoc, and R.I. Tanner, *J. Fluid Mech.*, **98**, 253 (1980).

(23) E. Ben-Sabar, and B. Caswell, *J. Rheology*, **25**, 537 (1981).

(24) H. Nguyen, and D.V. Boger, *J. Non-Newt. Fluid Mech.*, **5**, 353 (1979).

(25) M.A. McClelland, and B.A. Finlayson, AIChE *Annual Meeting, Paper* 90g (1985).

(26) K.R. Reddy, and R.I. Tanner, *J. Rheology*, **22**, 661 (1978)

(27) P.W. Chang, Th.W. Patten, and B.A. Finlayson, *Comp. Fluids*, **7**, 267 (1979).

(28) M.J. Crochet, and R. Keunings, *J. Non-Newtonian Fluid Mech.*, **7**, 199 (1980).

(29) C.J. Coleman, *J. Non-Newtonian Fluid Mech.*, **8**, 261 (1981).

(30) M.B. Bush, J. F. Milthorpe and R. I. Tanner, *J. Non-Newtonian Fluid Mech.*, **16**, 37 (1984).

(31) M.B. Bush, *J. Non-Newtonian Fluid Mech.*, **34**, 15 (1990).

(32) S. Middleman, and J. Gavis, *Phys. Fluids*, **4**, 355 (1981).

(33) Z. Tadmor, and C.G. Gogos, *"Principle of Polymer Processing,"* John Wiley and Sons, New York, pp. 534 (1979).

(34) B. Yang, and L.J. Lee, *Polym. Eng. Sci.*, **27** (14), 1088 (1987).

(35) K. Oda, J.L. White, and F.S. Clark, *Polym. Eng. Sci.*, **18**, 25 (1978).

(36) C.D. Han, and Y.W. Kim, *Trans. Soc. Rheol.*, **19** (2), 245 (1975).

(37) R.A. Mendelson, and F.L. Finger, *J. Appl. Polym. Sci.*, **19**, 1061 (1975).

(38) R.N. Shroff, and M. Shida, *Soc. Plastic Engrs*. ANTEC Preprints, Montreal, April 1977.

(39) I. Shida, T. Masuda, and S. Onogi, Preprints 21st *Rheology Symphosium*, Fukui, Japan, October 1973.

(40) H.M. Laun, and H. Schuch, *J. Rheology* **33**, 119 (1989).

(41) J. Vlachopoulos, and T.W. Chan, *J. Appl. Polym. Sci.*, **21**, 1177 (1977).

(42) A.B. Metzner, E.L. Carley, and I.K. Park, *Modern Plastics*, **37** (11), 133 (1960).

(43) E.B. Bagley, S.H. Storey, and D.C. West, *J. Appl. Polym. Sci.*, **7**, 1661 (1963).

(44) C.D. Han and M. Charles, *Trans. Soc. Rheol.*, **14** (2), 213 (1970).

(45) N. Nakajima, and M. Shida, *Trans. Soc. Rheol.*, **10**, 299 (1966),

(46) W. Philippoff, and F.H. Gaskins, *Trans. Soc. Rheol.*, **2**, 263 (1958).

(47) E.B. Bagley, *Trans. Soc. Rheol.*, **5**, 355 (1961).

(48) R.A. Mendelson, and F.L. Finger, *J. Polym. Sci.*, Part-C, **35**, 1177 (1971).

(49) J. Vlachopoulos, M. Horie, and S. Lindorikis, *Trans. Soc. Rheol.*, **16** (4), 669 (1972).

(50) J. Vlcek, *Rheol. Acta*, **21**, 460 (1982).

(51) C.W. Macosko, "*Rheology Principles Measurements and Application*," Wiley-VCH, New York, Ch. **6**, 236 (1990).

(52) N.R. Kumar, A.K. Bhowmick, and B.R. Gupta, *Kautschuk Gummi Kunststoffe*, **45**, 531 (1992)

(53) J. E. Pritchard, "*Modern Plastics Encyclopedia*," Phillips Petroleum Com. pp. 28 (1966).

(54) J. E. Pritchard, "*Modern Plastics Encyclopedia*," Phillips Petroleum Com. pp. 29 (1966).

(55) J. E. Pritchard, "*Modern Plastics Encyclopedia*," Phillips Petroleum Com. pp. 30 (1966).

(56) www.dow.com/webapps/lit/litorder.asp?filepath=automotive/pdfs/noreg/301-02671.pdf&pdf=true

(57) J. Brandrup, and E. H. Immergut, "*Polymer Handbok*," 3rd Edn., John wiley and Sons Inc (1989).

(58) A.A. Collyer, and D.W. Clegg, "*Rheological Measurements*," 2nd Edn., London, Chapman & Hall (1998).

(59) B. Earnst, P. Navard, and J.M. Haudin, *J. Poly. Sci.*, Part-C *Poly. Letts.*, **25**, 79 (1987).

(60) Y. Mori, and K. Funatsu, *Appl. Poly. Symposium* **No. 20**, 209 (1973).

(61) A.S. Lodge, "*Elastic Liquids*," Academic Press, New York, pp. 131 (1964).

(62) A.S. Lodge, D.J. Evans, and D.B. Scully, *Rheol. Acta*, **4**, 140 (1955).

(63) A. Kaye, *Coll. Aeronautics*, Cranfield, Notes, **No. 134** (1962).

(64) B. Bernstein, E. Kearsley, and L. Zapas, *Trans. Soc. Rheol.*, **7**, 391 (1963).

(65) B. Bernstein, *Acta Mech.*, **2**, 329 (1960).

(66) A. Jeffrey, "*Engineering and Scientists*," Nelson and Sons Ltd. Australia, South Africa and Canada, pp. 240 (1976).

(67) J.L. White and A. Kondo, *J. Non-Newtonian Fluid Mech.*, **3**, 77 (1977).

(68) J.L. White, *Trans. Soc. Rheol.*, **18**, 271 (1975).

(69) J.D. Ferry, *Viscoelastic Properties of Polymers*, 2nd Edn., Wiley, New York, 1970.

(70) J.P. Rothstein, and G.H. McKinley, *J. Non-Newtonian Fluid Mech.*, **86,** 61, (1999).

(71) D. Huang, and G.B. McKenna, *J. Chem. Phys.*, **14** (13), 5621 (2001).

(72) P.J. Carreau, D.C.R. DeKee, and R.P. Chhabra, *"Rheology of Polymetric Systems,"* Hanser Publishers, New York pp. 51 (1997).

(73) D. Huang, and G.B. McKenna, *J. Chem. Phys.*, **114** (13), 5621 (2001).

(74) M. Matsui, and D.C. Bogue, *Trans. Soc. Rheol.*, **21** (1), 133 (1977).

(75) T. Matsumoto, and D.C. Bogue, *Trans. Soc. Rheol.*, **21** (4), 453 (1977).

(76) R.G. Griskey, *"Polymer Processing Engineering,"* Chapman and Hall Publishers, New York pp. 109 (1995).

(77) J. M. Dealy, and K.F. Wissbrun, *"Melt rheology and its role in plastics processing,"* Van Vostrand Reinhold, New York pp. 399 (1999).

(78) C.W. Macosko, *"Rheology,"* VCH Publishers, New York pp. 84 (1994).

(79) R.G. Griskey, *"Polymer Processing Engineering,"* Chapman and Hall Publishers, New York pp. 114 (1995).

(80) F. Bueche, *J. Chem. Phys.*, **22,** 1570 (1954).

(81) C.W. Macosko, *"Rheology,"* VCH Publishers, New York pp. 93 (1994).

(82) C.W. Macosko, *"Rheology,"* VCH Publishers, New York pp. 86 (1994).

(83) P.J. Carreau, *Ph. D. Thesis*, Univ. of Wisconsin (1969)

(84) J. M. Dealy, and K.F. Wissbrun, *"Melt rheology and its role in plastics processing,"* Van Vostrand Reinhold, New York pp. 162 (1999).

(85) F. Bueche, and S.W. Harding, *J. Polym. Sci.*, **32,** 177 (1958).

(86) C.W. Macosko, *"Rheology,"* VCH Publishers, New York pp. 95 (1994).

(87) W.G. Kumar, *J. Polym. Sci.*, "Macromolecule Review," **15,** 255 (1980).

(88) C.W. Macosko, *"Rheology,"* VCH Publishers, New York pp. 96 (1994).

(89) D. W. Van Krevelen, *"Properties of Polymers,"* Elsevier Scientific Publishing Company, New York pp. 348 (1976).

(90) T. Arai, and H. Aoyama, *Trans. Soc. Rheol.*, **7**, 333 (1963).

(91) L. E. Neilsen, "*Polymer Rheology*," Marcel Dekker Inc., New York (1977).

(92) M. G. Roger, *J. Appl. Polym. Sci.*, **14**, 1679 (1970).

(93) N. Minagawa, and J. L. White, *J. Appl. Polym. Sci.*, **20**, 501 (1976).

A 143512